CHEMISTRY
A European Journal

Supporting Information

Magnetically Aligned Supramolecular Hydrogels

Matthew Wallace,*[a] Andre Zamith Cardoso,[a] William J. Frith,[b] Jonathan A. Iggo,[a] and Dave J. Adams*[a]

chem_201405500_sm_miscellaneous_information.pdf

SUPPORTING INFORMATION

1. Confocal Microscopy:

1.1. Sample preparation

All samples were prepared in D_2O in order to be fully comparable with the NMR experiments.

For the samples of Figs. 1c, 2c,d, 0.5 wt% solutions of NapFF were prepared as for the NMR analysis but with the NapFF dissolved in a solution containing approximately 0.002 mg/mL Nile blue dye which was prepared by dilution of a 0.01 mg/mL stock solution. For the gel samples on Fig. 2c,d, 900 μL of the NapFF solutions were transferred after mixing to 35 mm glass-bottom cell culture dishes (Greiner-Bioone) and left to stand for 6 days away from the magnetic field. To prepare gels, $CaCl_2$ solution (52 mg/mL, 40 μL) was added drop-wise to a small region on the side of the dish. Prior to addition of $CaCl_2$, the sample to be gelled in a 9.4 T NMR magnet (Fig. 2c) was first lowered down the bore of the spectrometer and left to stand in the field for one hour before it was raised, the $CaCl_2$ added, and the sample carefully lowered back into the field. Samples were left to stand overnight before imaging. Care was taken to ensure that the sample dishes were level until gelation was complete. For the high pD solution in Fig. 1c, the solution of NapFF was instead transferred to a 5 mm NMR tube and aged for 6 days prior to imaging.

For the gel samples of Fig. S28, a 0.1 mg/mL suspension of Nile blue was prepared and stirred overnight before being passed through a 1 μm filter. The filtrate was diluted by a factor of 2.5 and used to prepare an 0.5 wt% solution of NapFF which was placed in 4 mL aliquots into 12 mL polypropylene syringes. The syringe barrels had been cut off near the top to give a tube while the plungers had been shortened in order to allow the syringes to fit in a home-built cradle which served to keep the samples vertical as they were lowered in/out of the magnetic field. After addition of the NapFF solution, the syringes were sealed with Parafilm and left to age away from the magnetic field for six days. To prepare gels, $CaCl_2$ solution (200 mg/mL, 114 μL) was added dropwise over the top of the NapFF solution and the syringes sealed with Parafilm. Samples were left to stand for ca. 60 hours before analysis. As with the

sample of Fig. 2c, the sample to be prepared in a 9.4 T magnetic field was exposed to the field for one hour prior to the addition of $CaCl_2$, whereupon the sample was promptly placed back in the field.

1.2. Confocal imaging

Confocal microscopy images were taken using a Zeiss LSM 510 Meta confocal microscope. Fluorescence from Nile blue was excited using a 633 nm Helium-Neon laser and emission detected above 650 nm.

The images in Fig. 2c,d, were obtained with the lid of the dish removed, while Fig. 1c was obtained by imaging directly through the NMR tube. It was not possible to image gels in 5 mm NMR tubes as the resolution imposed by the curved glass surface and the thickness of the sample was found to be insufficient for the observation of any structures. To obtain the images in S28 and S29, the gels were extruded from the syringes using the plunger and cut into ca. 2 mm thick slices, both perpendicular and parallel to the direction at which the 9.4 T magnetic field had been applied to the sample gelled in the field, using a fresh scalpel blade. Due to syeneresis of the gel, it was possible to extrude the gel without damage. The gel slices were transferred, immediately after cutting, to 35 mm glass-bottom cell culture dishes and imaged. The top 5 mm of the gels were discarded to ensure that only the part of the sample which had been gelled by the downward diffusion of $CaCl_2$ was studied.

2. NMR:

All NMR experiments were performed at (298±0.5) K. All ^1H and ^2H NMR experiments, unless otherwise stated, were performed on a Bruker Avance II 400 MHz (^1H) wide bore spectrometer operating at 400.20 MHz for ^1H and 61.43 MHz for ^2H. Z-gradients were applied using a Bruker TBI-W1 probe controlled by a Bruker GREAT 10 A gradient driver delivering a maximum gradient intensity of 55 G/cm. Spectra recorded at 4.7 T (200 MHz ^1H) were recorded on a Bruker AMX II 200 or Bruker Avance I spectrometer operating at 30.72 MHz for ^2H. ^2H spectra of D_2O were recorded *via* the lock channel with 4096 data points, a 200 μs pulse ($\pi/2$), a sweep width of 10 ppm and a relaxation delay of 1.0 s. 8 transients were acquired giving a total acquisition time of 35 seconds. ^2H spectra of dioxane-d_8 and other deuterated

probe molecules at 0.05 vol% were recorded with presaturation applied to the D_2O resonance during the relaxation delay (1.0 s) followed by a spoil gradient (27 G/cm, 1 ms) to dephase any observable magnetisation before the $\pi/2$ pulse and data acquisition. 3072 data points were collected in 1024 transients giving a total acquisition time of 1 hour. After data acquisition, the FID was manually inspected and trimmed prior to Fourier transformation in order to maximise the signal to noise ratio of the solute resonance. More concentrated samples required fewer scans.

All chemical shift imaging experiments were performed using a gradient phase encoding sequence based on that presented by Trigo-Mouriño et al.[1] ($\pi/2$ - τ_1 - g - τ_2 - Acquire, where g is a gradient pulse in the form of a smoothed square and τ_1 and τ_2 are delays of length 10 μs and 200 μs respectively). For ^{2}H-NMR images, g was varied linearly in 128 steps from -52 to 52 G/cm with a pulse duration of 816 μs. 3072 data points were collected in one transient at every step with a sweep width of 10 ppm, giving a total experimental time of 6 minutes and a theoretical spatial resolution of 203 μm. For ^{1}H images, g was varied linearly in 128 steps from -27 to 27 G/cm with a pulse duration of 238 μs. 4096 data points were recorded in one transient at each step with a sweep width of 10 ppm and a relaxation delay of 2.2 s, giving a total acquisition time of 6 minutes and a spatial resolution of 203 μm. Pre-saturation of the residual solvent resonance (HOD) was applied during the relaxation delay to ease the task of phasing the 2D datasets and to allow the observation of NapFF resonances close to this peak. Images were obtained after 2D Fourier transformation of the raw datasets followed by 2D phase correction. No zero filling was applied in the gradient dimension. ^{1}H images were Fourier transformed with 8192 points in the direct dimension with an exponential window function applied, giving a line broadening of 3 Hz. ^{2}H images of D_2O were Fourier transformed with 16384 points in the direct dimension. No line broadening factor was applied to ^{2}H images or spectra. ^{2}H images of deuterated probe molecules were processed as for the images of D_2O but Fourier transformed in the gradient dimension with a sine function applied.

3. SEM, FTIR and Powder X-Ray Diffraction:

3.1. Sample Preparation

The same hydrogel samples were used for SEM, FTIR and Powder X-Ray Diffraction (pXRD). To prepare these samples, a 0.5 wt% NapFF solution in D_2O was prepared

and transferred in 3.5 mL aliquots to 12 mL polypropylene syringes, which had been prepared as described for the confocal imaging experiments, and allowed to age away from the magnetic field for six days. To prepare $CaCl_2$-triggered hydrogels, $CaCl_2$ solution (200 mg/mL, 100 μL) was added dropwise over the surface of the NapFF solution. For GdL-triggered hydrogels, solid GdL (19 mg) was sprinkled over the surface of the NapFF solution. For samples to be gelled in the 9.4 T magnetic field, the NapFF solutions were placed in the field for one hour prior to the addition of the gelation trigger whereupon they were promptly sealed and returned to the magnetic field. Samples were exposed to the magnetic field for 50 hours and stood away from the magnetic field for a further 20 hours prior to analysis.

Syneresis of the gels made it possible to extrude the gels from the syringes without significant damage. For analysis, the gels were extruded from the syringes and the extruded section cut with a fresh scalpel blade before being transferred for analysis. The top 5 mm of each sample was discarded to avoid artefacts due to the initially very high concentration of gelation trigger in this region.

3.2. Scanning Electron Microscope (SEM)

SEM images were recorded using a Hitachi S-4800 FE-SEM at 1 KeV. Silicon wafers were used to dry and probe the hydrogels. The 2 mm (height) x 15 mm (diameter) circular $CaCl_2$ hydrogels were placed on the silicon wafers with the plane of the circle lying perpendicular to the axis of the magnetic field when the magnetically aligned gels were prepared. The gels were dried with both a minimal nitrogen flow for 2 hours or alternatively blotting for 20 minutes with a filter paper. A selection of representative images was taken from over 60 images across each sample. This was done to minimize the drying artifacts in the sample microstructure. To avoid charging effects, after drying the samples were Au coated for 1 min at 10 mA using a sputter-coater (EMITECH K550X) prior to imaging. With this coating, a minimal 5 nm Au layer was deposited on top of the sample. Imaging was conducted with a low voltage mode (1 keV) at a 1.5 to 3 mm distance from the sample and a deceleration mode (i.e. deceleration voltage of 1.5 keV, from 2.5 to 1 keV).

3.3. Fourier transform infrared spectroscopy (FTIR)

A FTIR liquid transmission cell (OMNI Cell System, Specac) was used for all measurements. The samples were contained between two CaF_2 windows (thickness, 4

mm) separated by a 0.1 mm PTFE spacer. The hydrogels were cut to make a cylinder with approximately 15 (diameter) x 2 mm (height) from the syringe and subsequently deposited in the FTIR liquid cell. D_2O was used as the solvent for all the infrared spectral measurements. The NapFF solutions analysed by FTIR were freshly mixed in order to avoid any artefacts due to the shearing of aged solutions upon transferal to the IR cell. The CaF_2 windows and spacer were sealed together with Parafilm and the solution placed inside using a pipette. The sample was then placed inside the 9.4 T magnetic field of an NMR spectrometer for one hour before being mounted in the IR cell and the spectrum recorded. The procedure was then repeated but without the solution being exposed to the magnetic field. It was not possible to adequately seal the windows together so that NapFF solution could be aged inside.

FTIR spectra were acquired using a Bruker Vertex spectrometer. A spectrum was obtained from averaging 64 scans between 4000 and 700 cm^{-1} with a spectral resolution of 2 cm^{-1}. A D_2O background was obtained before each set of measurements.

3.4. X-Ray Powder Diffraction

A 'background' sample for $CaCl_2$-triggered hydrogels was prepared by drying a solution containing 0.012 M NaOH and 0.05 M $CaCl_2$ in air. Hydrogels (3 block of approximately 2 x 4 x 5 mm) and the calcium crystals were dried in the aluminium holder over 7 hours in air before the measurements.

Powder X-ray diffraction data were collected on a PANalytical X'pert pro multipurpose diffractometer (MPD) in transmission Debye−Scherrer geometry operating with a Cu anode at 40 kV and 40 mA. PXRD patterns were collected in 1 h scans with a step size of 0.013° 2θ and a scan time of 115 s/step with 2θ range between 4 − 35°. The incident X-ray beam was conditioned with 0.04 rad Soller slits and an anti-scattering slit of 0.5°. The diffracted beam passed through 0.04 rad Soller slits before being processed by the PIXcel2 detector operating in scanning mode.

4. Figures

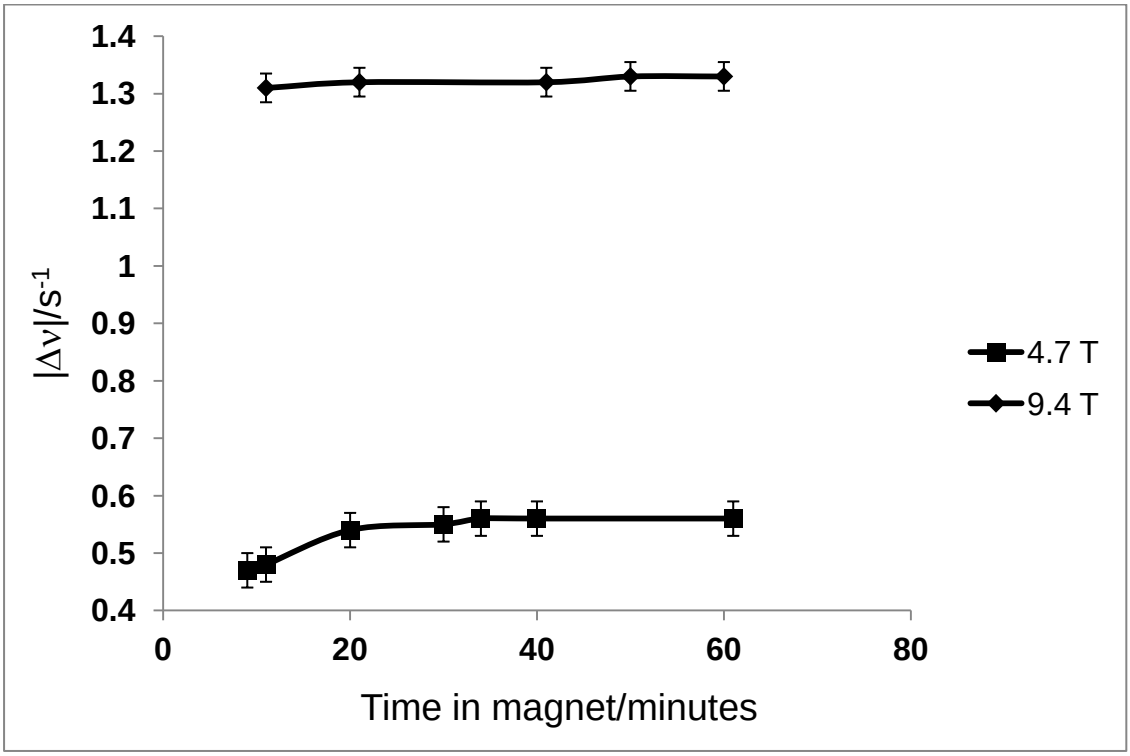

Figure S1. Plot of the residual quadrupolar coupling (|Δν|) exhibited by the D_2O resonance in 0.5 wt% solutions of NapFF at pD 12.6 at different field strengths as a function of exposure time in the magnetic field. A standard error in |Δν| of ±0.03 Hz has been assumed. The black lines are to guide the eye.

The dead time at the start of the experiment is the time taken to obtain a shim on the sample of sufficient quality for accurate determination of RQCs. The samples at both field strengths came from the same preparation of NapFF solution.

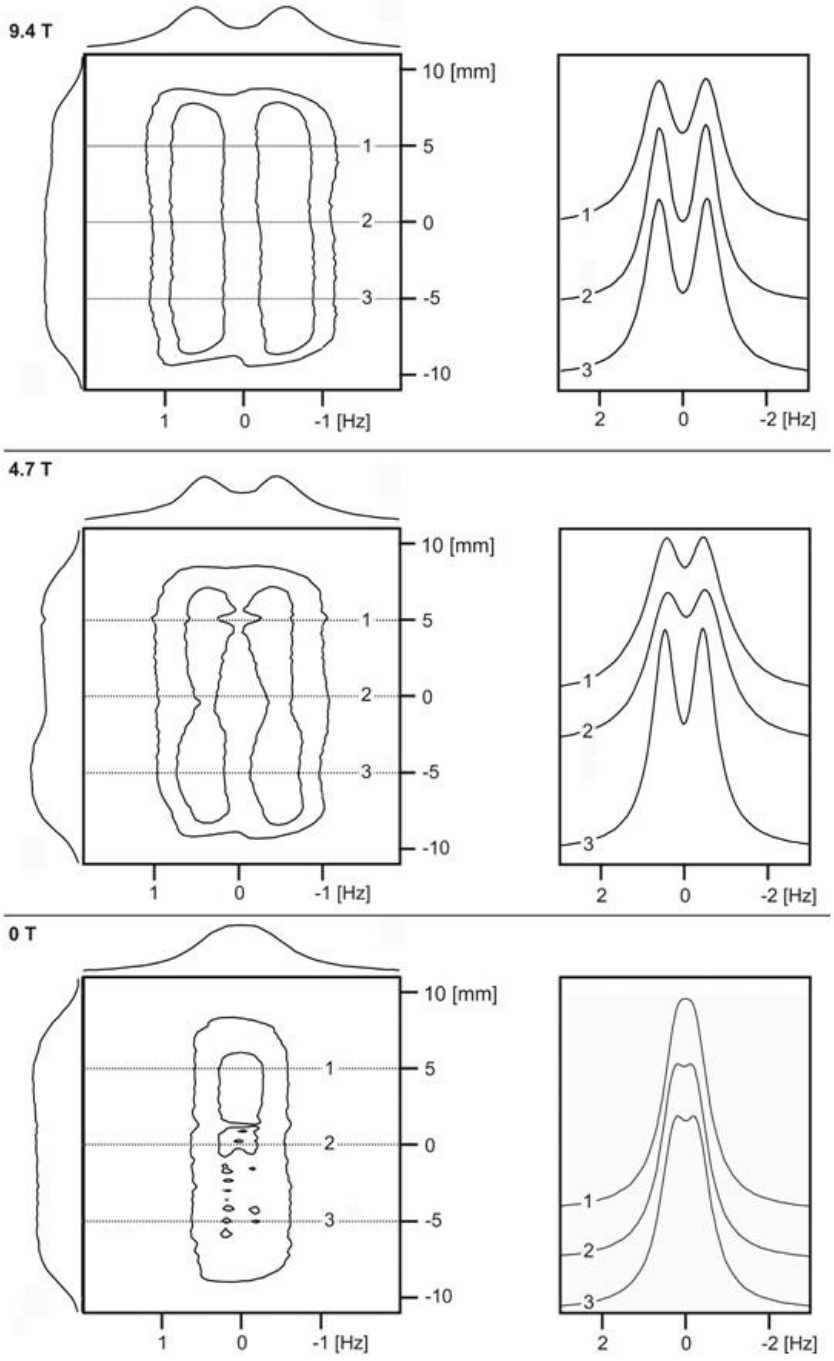

Figure S2. Chemical shift images of $CaCl_2$ triggered gels prepared at 9.4 and 4.7 and 0 T. 0 T denotes a gel prepared away from a strong magnetic field. The images are presented as 2D contour plots (left) with spectra (right) extracted from the positions indicated by dashed lines.

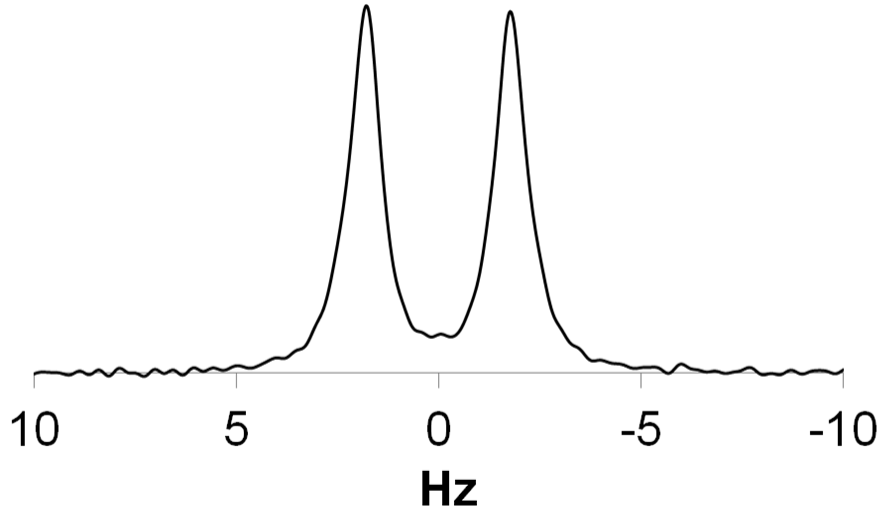

Figure S3. ^{2}H spectrum of dioxane-d_8 in an 0.5 wt% NapFF $CaCl_2$-triggered hydrogel.

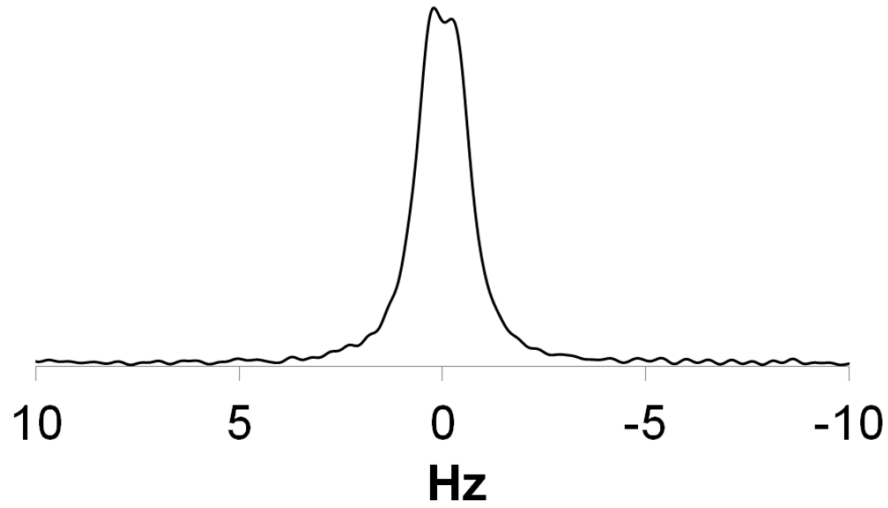

Figure S4. ^{2}H-NMR spectrum of dioxane-d_8 in a 0.5 wt% solution of NapFF at pD 12.6.

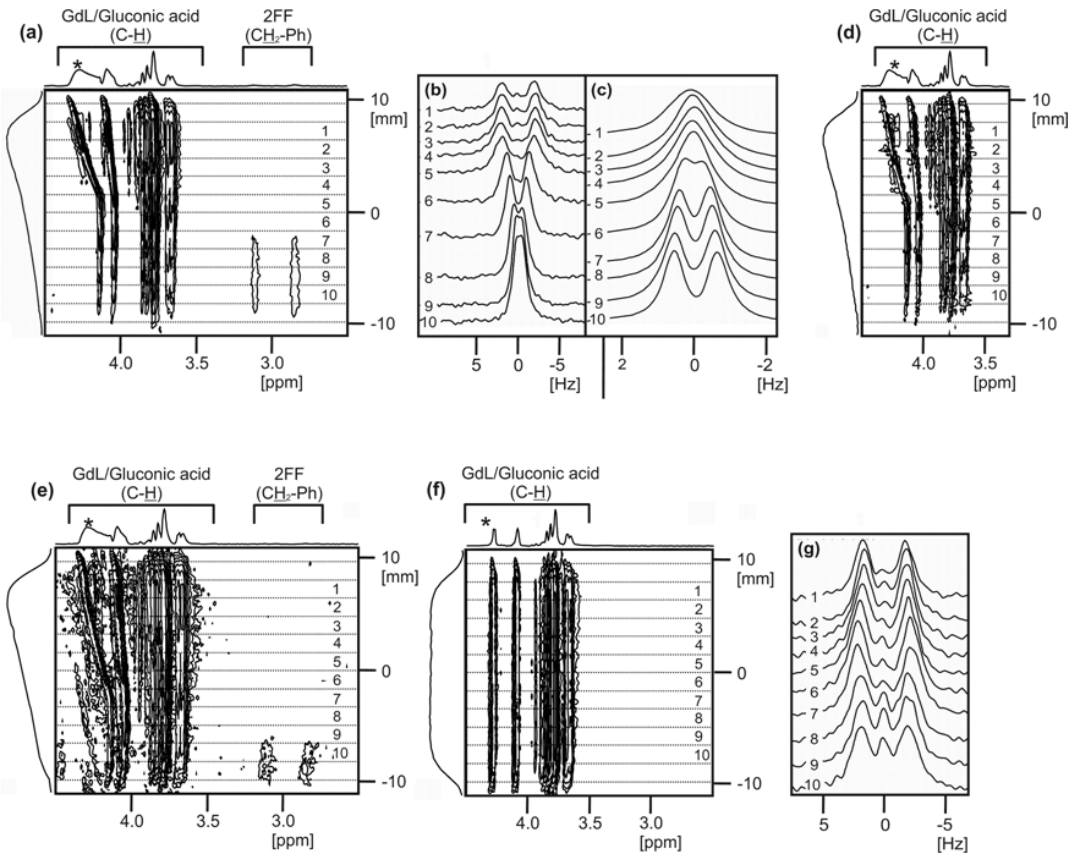

Figure S5. Following the formation of a GdL-triggered NapFF gel by chemical shift imaging (CSI) (a) ^{1}H image of sample to show GdL/gluconic acid peaks and NapFF resonances. The projection on the left indicates the concentration gradient of the GdL. The signal falls away towards the top of the image due to the finite size of the radiofrequency coil of our instrument. It is possible to estimate the pD *in situ* from the chemical shift of the gluconic acid peak marked *.[2] It can thus be inferred that the pD at and above region 5 is ≤ 7 and so, given a pK_a of NapFF of 6,[3] the fibres will be protonated to a significant degree. (b) ^{2}H-NMR spectra of dioxane-d_8 at regions indicated on (a). The magnitude of the RQC exhibited gradually increases as the pD falls. Above region 5, a singlet peak becomes visible between the doublet indicative of an isotropic phase. (c) ^{2}H-NMR spectra of D_2O at regions indicated on (a). The RQC of D_2O gradually diminishes to zero as the pD falls. (d) ^{1}H image of sample showing how little GdL had progressed down tube since (a) was recorded. Images (a)-(d) were recorded in alphabetical order. (e) ^{1}H image of sample before removal from magnetic field. NMR-visible NapFF is apparent at the base of the image indicating this region of the sample had not yet gelled fully. (f) ^{1}H image of sample on (e) after ageing away from magnetic field for two weeks. No residual concentration gradient of the GdL/gluconic acid is apparent and the pD appears uniform throughout the

sample. (g) ^{2}H-NMR spectra of dioxane-d_8 at regions indicated on (e) and (f) in the sample after ageing for two weeks away from magnetic field. The singlet (isotropic) peak is noticeably larger in the lower portion of the sample (regions 9 and 10) where the sample had not completely gelled prior to removal from the magnetic field.

Images (b), (c) and (g) were recorded with 16 gradient steps giving a theoretical resolution of 1.6 mm. (b) and (g) were recorded with pre-saturation applied to the D_2O resonance along with a spoil gradient to de-phase any observable magnetisation generated. For (b), 256 scans were recorded at each gradient step with 2048 data points giving a total acquisition time of 3 hours while for (g) 1024 scans were recorded at each step giving a total acquisition time of 13 hours.

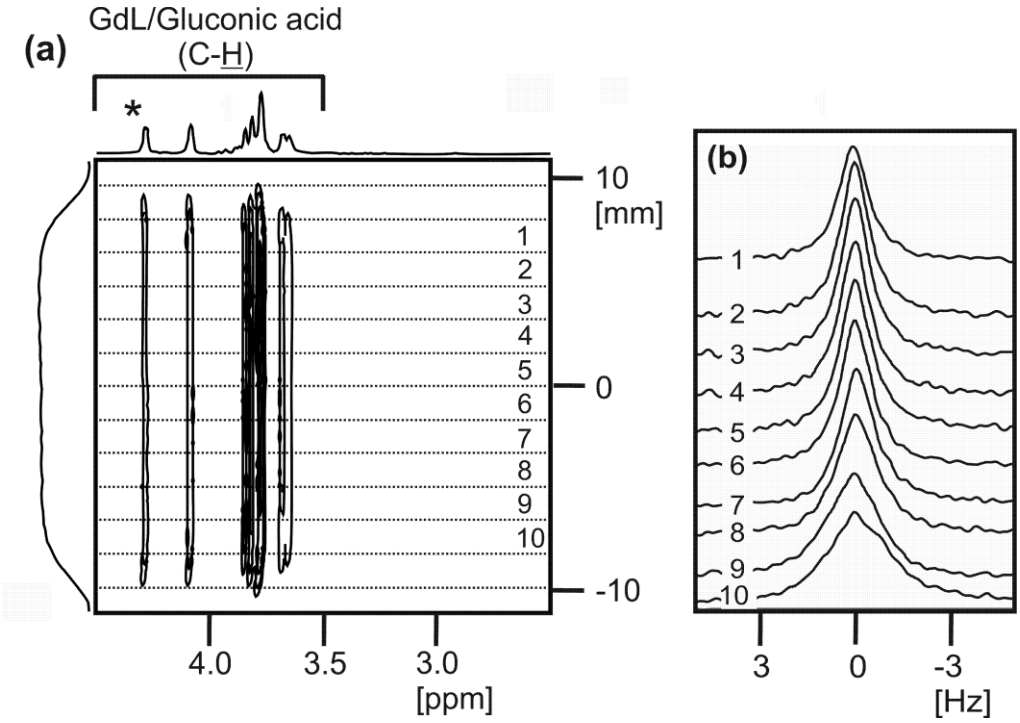

Figure S6. CSI images of the GdL-triggered NapFF gel of Fig. 2b prepared in a water bath away from the magnetic field. (a) ^{1}H image of sample recorded two weeks after addition of GdL to NapFF solution showing that the GdL/gluconic acid concentration and pD are uniform throughout the sample. (b) ^{2}H-NMR spectra of dioxane-d_8 at regions indicated on (a). No RQC is detectable indicating that the gel cannot re-orient in the magnetic field.

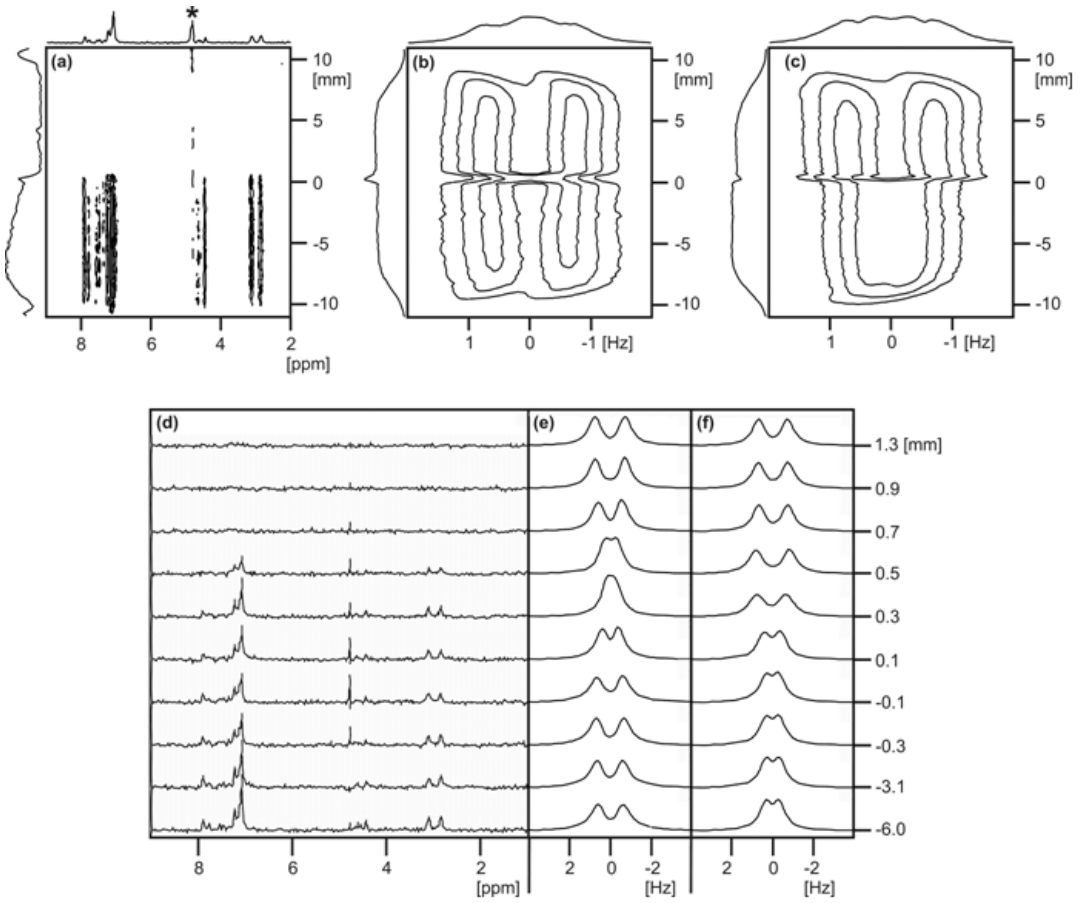

Figure S7. Following the formation of a $CaCl_2$-triggered NapFF hydrogel by CSI. (a) ^1H image of the sample of Fig. 3a, taken immediately before the ^2H image. The residual signal from HOD is marked *. All other resonances belong to NapFF. (b) Fig. 3a, reproduced here for convenience: ^2H image of D_2O resonance in sample taken immediately before removal from magnetic field. (c) Fig. 3b, reproduced here for convenience: ^2H image of D_2O resonance in sample after ageing away from magnetic field for two weeks. (d) Extracted ^1H spectra from (a) at vertical positions indicated on left of figure. (e) Extracted 2H spectra from (b) at vertical positions indicated. (f) extracted spectra from (c)

The ^1H resonances of the NMR-visible NapFF in solution in the absence of Ca^{2+} (a), (d) – measured as 50±10 % of the total NapFF present with respect to an internal capillary in NapFF solutions with no Ca^{2+} present – all vanish at approximately the same point at which the RQC of D_2O temporarily diminishes to almost zero (b), (e). The loss of the ^1H signal from the NMR-visible NapFF is attributable to the formation of Ca^{2+}-coordinated species, which are presumably insoluble and therefore not NMR-

visible. The temporary decrease in the RQC of D_2O is attributable to the presence of a mixture of NapFF-Ca^{2+} and NapFF-Na^{+} coordination sites for D_2O which averages the RQC almost to zero.[4] The transformations taking place as a solution of NapFF at high pH is transformed to a $CaCl_2$-trigered gel are the subject of ongoing investigations.

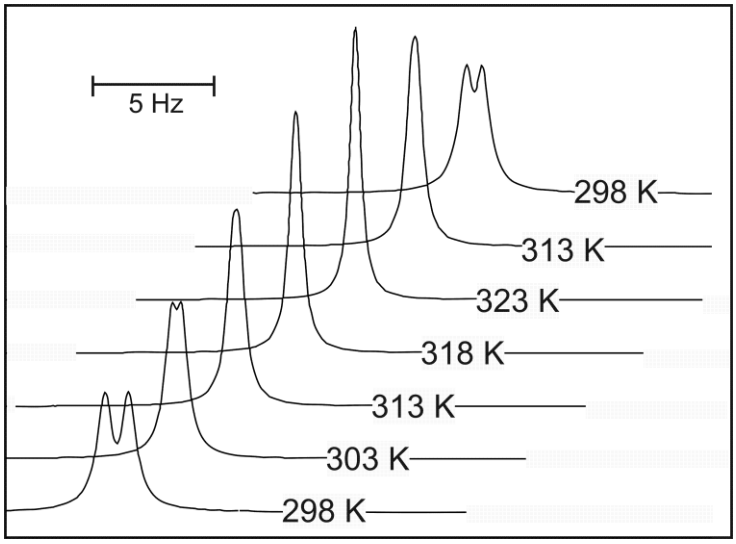

Figure S8. Effect of temperature on the RQC of D_2O in an 0.5 wt% solution of NapFF. ^2H spectra of D_2O at temperature shown are displayed on a staggered plot.

The RQC of D_2O decreases as the temperature is increased up to 323 K at which the resonance is a single sharp Lorentzian peak. Upon cooling down to 298 K there is an apparent hysteresis, the RQC being only 0.6 Hz compared to 1.0 Hz prior to heating. These results suggest that heating to 323 K 'melts' the aligned wormlike structures to give an isotropic solution, which upon cooling adopts a different state to the starting solution.

The sample was equilibrated at each temperature for 40 minutes before the ^2H spectra were recorded. The sample temperature was controlled using a Bruker BVT3200 temperature control unit which had been calibrated using a thermocouple immersed in water in an NMR tube. The accuracy of the stated temperatures is ±0.5 K.

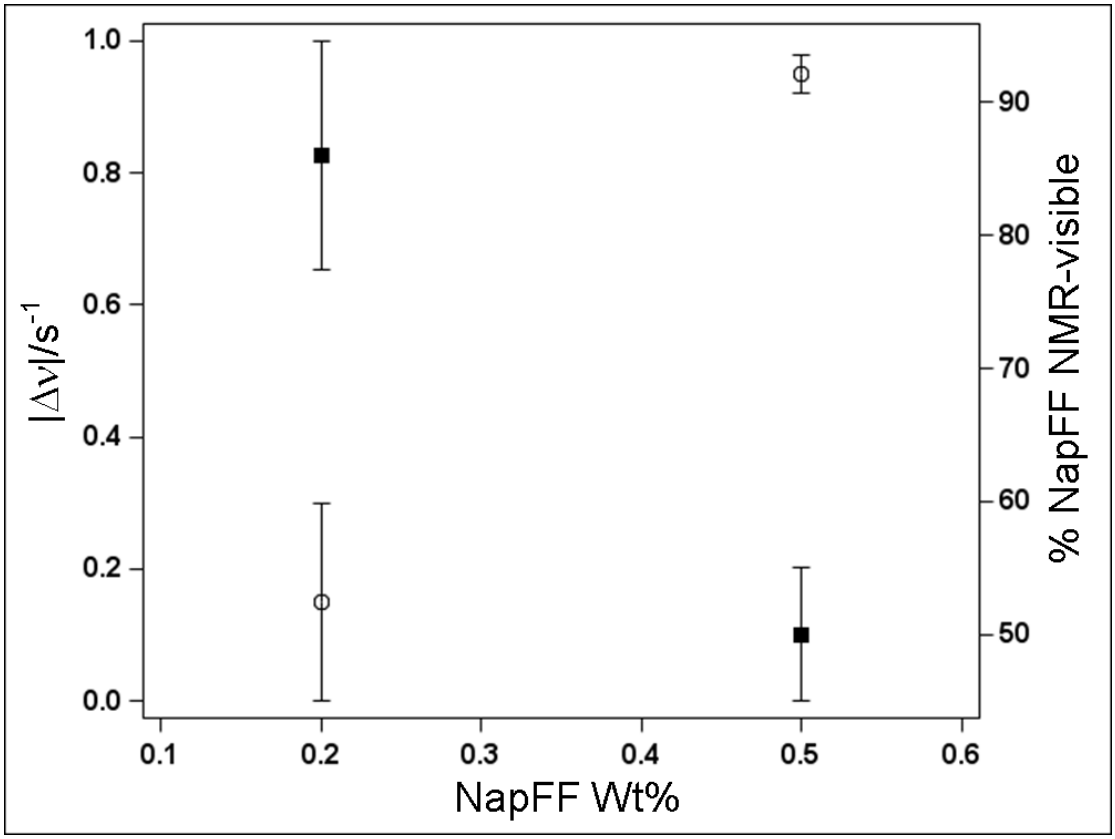

Figure S9. Plot of the RQC (|Δν|) of D_2O (circle) and the percentage of NMR-visible NapFF (square) in solutions of NapFF, versus the wt% of NapFF.

At 0.2 wt% NapFF, the RQC of D_2O is indiscernible, being less than the natural linewidth of the D_2O resonance. An error on this point of ±0.15 Hz has been derived based on a fitting of the resonance to Lorentzian doublets. An error of ±0.03 Hz has been assumed for the 0.5 wt% sample where the splitting is larger than the linewidth. The percentage of NapFF in the sample which is visible by ^{1}H-NMR was estimated by integrating the NapFF resonances (C$\underline{H_2}$-Ph) against the residual ^{1}H toluene resonance (methyl group) in an internal reference capillary filled with toluene-d_8. Prior to use, the capillaries had been calibrated using a 5 mg/mL sample of L-valine. A standard error of ±10% has been assumed in the determination of the percentage of ^{1}H-NMR visible NapFF. NapFF samples at 0.7 and 1.0 wt% were prepared but found unsuitable for analysis owing to the formation of dense liquid crystalline domains which seemingly sank to the bottom of the NMR tube as the sample was ageing (6-8 days) so that the RQC of D_2O was not homogeneous across the sample (Figure S17).

The above results suggest that worm-like structures which are not NMR-visible are required in order to align in the magnetic field and give rise to an RQC of D_2O. Such structures – in which the assembled molecules have a very low degree of mobility and consequently very short transversal relaxation times – seem to exist at concentrations below the limit at which an RQC can be resolved. The phase behaviour of NapFF in solution is the subject of ongoing work.

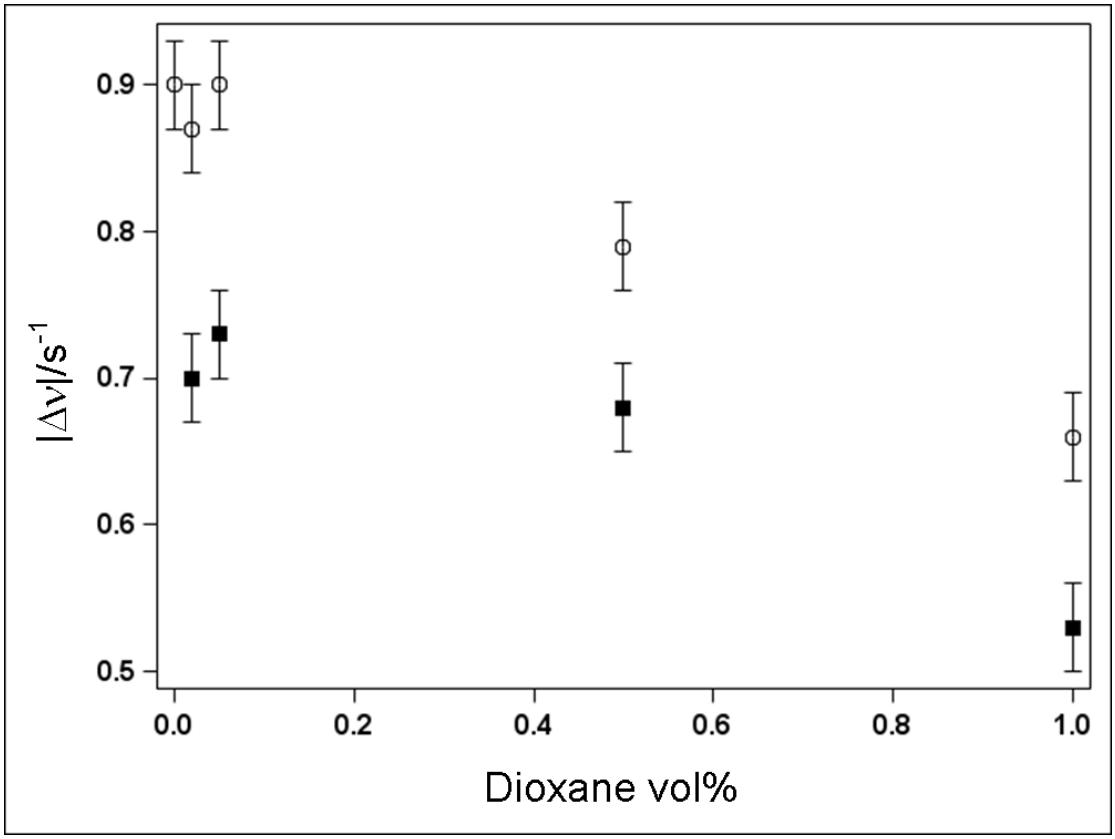

Figure S10. Plot of the RQC ($|\Delta\nu|$) of D_2O (circle) and 1,4-dioxane-d_8 (square) in 0.5 wt% solutions of NapFF versus the percentage of dioxane in the solution. Each solution was allowed to equilibrate in the magnetic field for at least 40 minutes before measurement of the RQCs, after which no significant changes in the RQCs took place. All samples were prepared from the same stock solution of NapFF. A standard error in $|\Delta\nu|$ of ±0.03 Hz has been assumed.

The RQCs of D_2O at 0.05, 0.02 and 0 vol% dioxane-d_8 are the same within error. At higher concentrations, the RQCs of both D_2O and dioxane decrease due to a change in the supramolecular organisation of the Nap-FF and/or increased competition for binding sites between dioxane molecules themselves and D_2O. In $CaCl_2$-triggered gels formed in the magnetic field – which unavoidably had to be prepared from different stock solutions of NapFF due to spectrometer availability – the RQCs of D_2O and dioxane were 1.2 Hz and 3.6 Hz respectively at 0.05 vol% dioxane and 1.4 Hz and 5.5 Hz at 0.5 vol% dioxane.

4. Other probes.

As well as dioxane-d_8, other water-soluble deuterated molecules can be used to study anisotropy in magnetically aligned NapFF hydrogels. CD_3CN and MeOD (CD_3OD) were chosen owing to their different properties. Formation of $CaCl_2$-triggered NapFF hydrogels incorporating these probes was then followed *in-situ* by CSI. Data for dioxane-d_8 is included for completeness. The concentration of all deuterated probe molecules was 0.05 vol%.

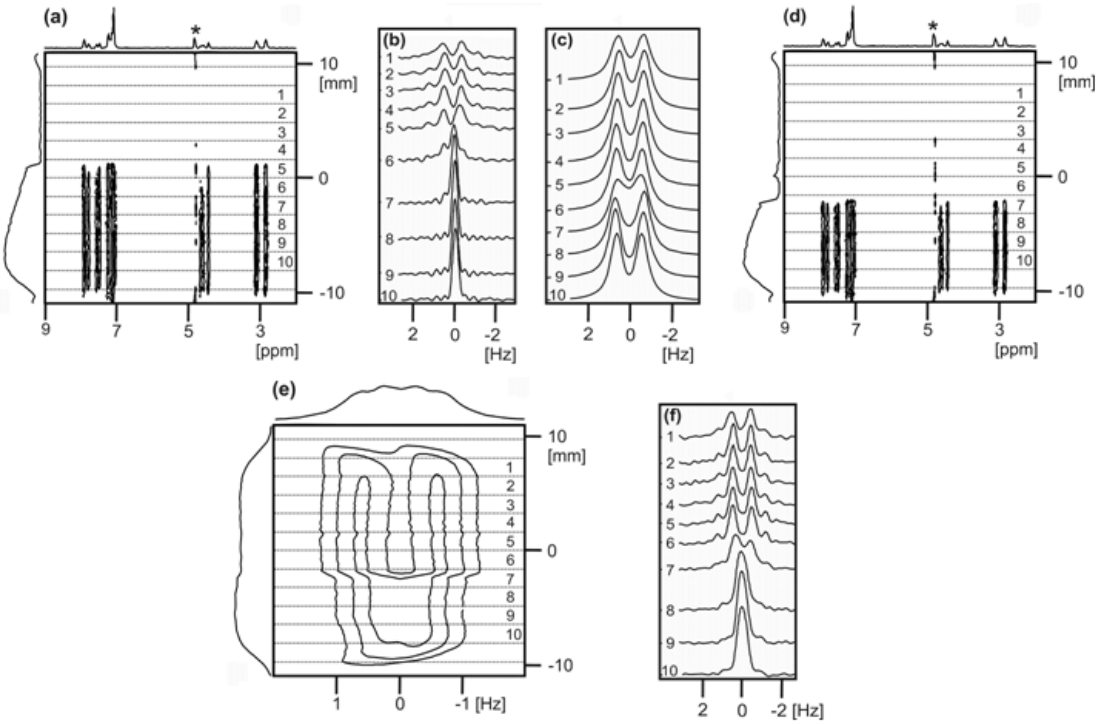

Figure S11. Use of CD_3CN as a probe molecule to follow formation of a $CaCl_2$-triggered 0.5 wt% NapFF hydrogel by CSI. (a) ^1H image of the sample taken before other images shown. The resonance marked * belongs to HOD, all other resonances belong to NapFF. (b) ^2H-NMR spectra of CD_3CN at regions indicated on (a) and (d). In the $CaCl_2$-triggered gel – above the 'front' where the signal from the NMR-visible NapFF disappears – the CD_3CN exhibits a clear splitting while in the 2FF solution below the 'front' the resonance is a singlet. The wiggles at the base of the spectra from regions 7-10 are due to truncation of the FIDs. (c) ^2H-NMR spectra of D_2O at regions indicated on (a) and (d). (d) ^1H image of sample to show how far $CaCl_2$ 'front' had progressed during the acquisition of (b). (e) ^2H image of D_2O in sample having aged in a water bath for eight days. (f) ^2H-NMR spectra of CD_3CN at regions indicated on (e). In the portion of the gel formed in the magnetic field, the CD_3CN

exhibits a clear splitting whereas in the portion gelled away from the field the RQC is less than the linewidth and cannot be resolved.

The observation that CD_3CN exhibits an RQC in a $CaCl_2$-triggered gel but not a solution of NapFF is attributable to the very different solvation environments around the NapFF structures present in both cases.

Images (b), (c) and (f) were recorded with 16 gradient steps giving a theoretical resolution of 1.6 mm. (b) and (f) were recorded with pre-saturation applied to the D_2O resonance along with a spoil gradient to de-phase any observable magnetisation generated. For (b), 256 scans were recorded at each gradient step with 4800 data points and a sweep width of 15 ppm giving a total acquisition time of 4 hours while for (f) 512 scans and 8192 data points were recorded at each step giving a total acquisition time of 12 hours.

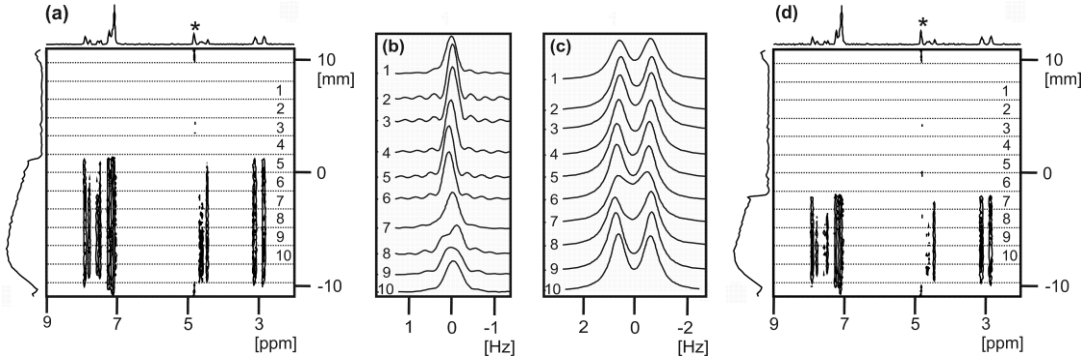

Figure S12. Use of MeOD as a probe molecule to follow formation of a $CaCl_2$-triggered 0.5 wt% NapFF hydrogel by CSI. (a) ^1H image of the sample taken before other images shown. The resonance marked * belongs to HOD, all other resonances belong to NapFF. (b) ^2H-NMR spectra of MeOD ($C\underline{D}_3$) at regions indicated on (a) and (d). The MeOD does not exhibit an RQC either in a solution of NapFF or in a $CaCl_2$-triggered gel. The wiggles at the base of the spectra from regions 1-8 are due to truncation of the FIDs. (c) ^2H-NMR spectra of D_2O at regions indicated on (a) and (d). (d) ^1H image of sample to show how far $CaCl_2$ 'front' had progressed during the acquisition of (b).

The lack of an observable splitting of the CD_3 group of MeOD is attributed to a relatively weak interaction between the hydrophilic molecule and the NapFF structures.

Images (b) and (c) were recorded with 16 gradient steps giving a theoretical resolution of 1.6 mm. (b) was recorded with pre-saturation applied to the D_2O resonance along with a spoil gradient to de-phase any observable magnetisation generated. 256 scans were recorded at each gradient step with 5530 data points and a sweep width of 15 ppm giving a total acquisition time of 5 hours.

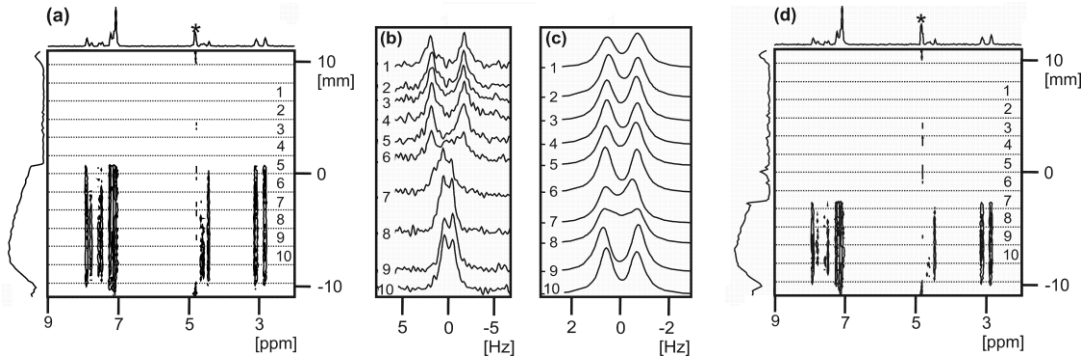

Figure S13. Use of dioxane-d_8 as a probe molecule to follow formation of a $CaCl_2$-triggered 0.5 wt% NapFF hydrogel by CSI. (a) ^1H image of the sample taken before other images shown. The resonance marked * belongs to HOD, all other resonances belong to NapFF. (b) ^2H-NMR spectra of dioxane-d_8 at regions indicated on (a) and (d). The dioxane exhibits an RQC both in solutions of NapFF and in $CaCl_2$-triggered gels (Fig. S3, S4), the latter being considerably larger. (c) ^2H-NMR spectra of D_2O at regions indicated on (a) and (d). (d) ^1H image of sample to show how far $CaCl_2$ 'front' had progressed during the acquisition of (b).

Images (b) and (c) were recorded with 16 gradient steps giving a theoretical resolution of 1.6 mm. (b) was recorded with pre-saturation applied to the D_2O resonance along with a spoil gradient to de-phase any observable magnetisation generated. 256 scans were recorded at each gradient step with 5530 data points and a sweep width of 15 ppm giving a total acquisition time of 5 hours.

5. Other Salts

It has previously been demonstrated that hydrogels can be formed upon the addition of a range of salts to 0.5 wt% solutions of NapFF.[5] $MgCl_2$ and NaCl were chosen to study the effect of the counterion on the gel formation process which was followed by chemical shift imaging (CSI). For both $MgCl_2$ and NaCl, the concentrations of salt and the procedure used to prepare gels were the same as used for $CaCl_2$-triggered gels, the final concentration of salt being 0.05 M.

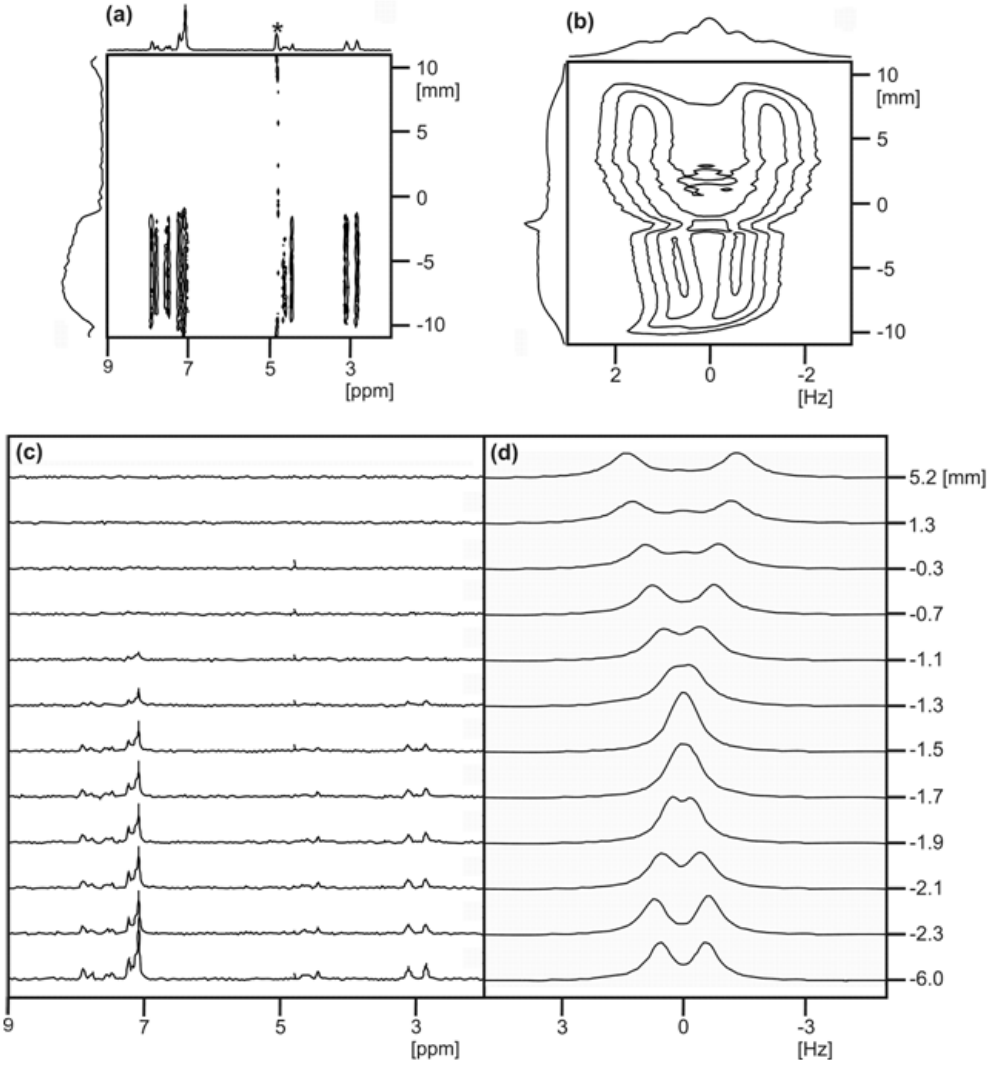

Figure S14. Following the formation of an $MgCl_2$-triggered 0.5 wt% NapFF hydrogel by CSI. (a) ^{1}H-image of sample. The resonance marked * belongs to HOD, all other resonances belong to NapFF. (b) ^{2}H-image of D_2O in sample, taken immediately after (a) was recorded. (c) ^{1}H spectra extracted from (a) at vertical position indicated. (d) ^{2}H spectra of D_2O extracted from (b) at vertical position indicated.

As with $CaCl_2$ (Fig. S7), the RQC of D_2O is indiscernible at around the position at which the ^1H signal from the NMR-visible NapFF disappears and is of appreciable magnitude both above and below this point – the salt diffusion 'front'. However, the RQC above the 'front' is considerably larger – 2.7 Hz compared to 1.4 Hz in the $CaCl_2$-triggered gel – and an additional singlet (isotropic) peak is apparent between the doublet peaks. These two observations are attributable to either a different structuring of D_2O around the NapFF fibres when Mg^{2+} is present, or a different gel microstructure compared to $CaCl_2$-triggered gels. It has previously been shown that $CaCl_2$ and $MgCl_2$-triggered hydrogels have similar mechanical properties.[5]

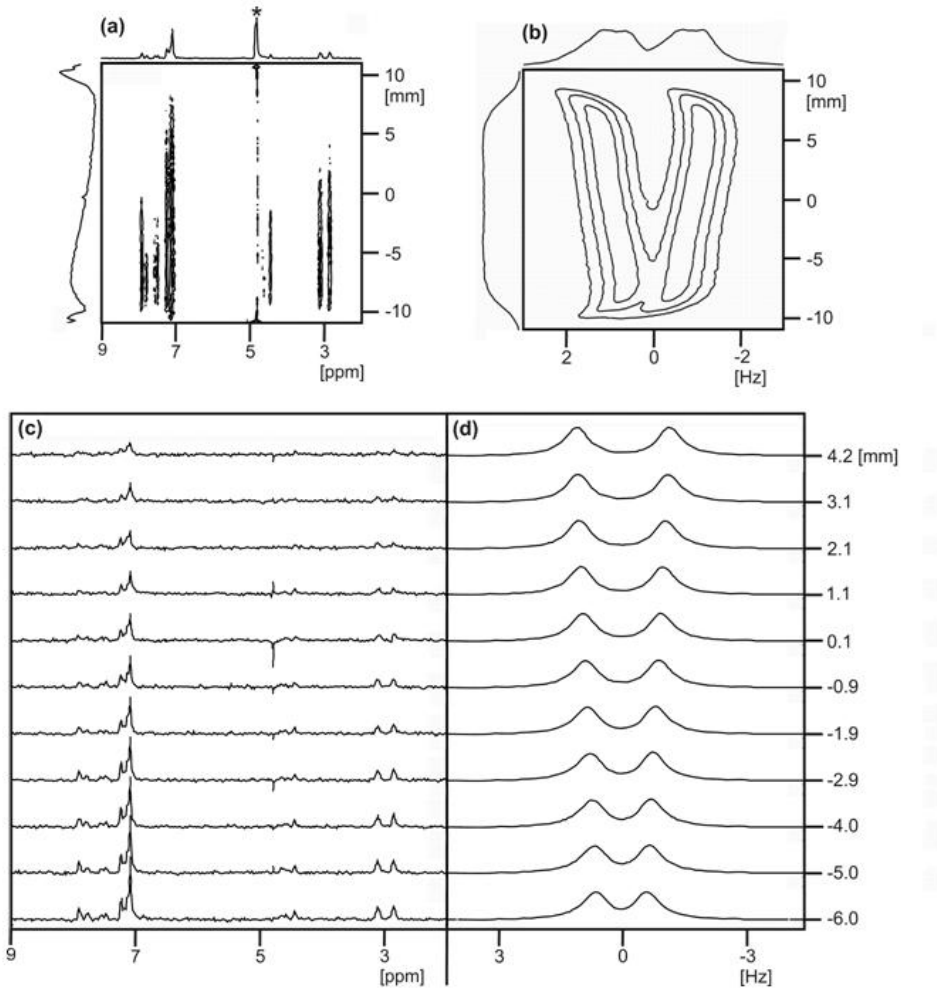

Figure S15. Following the formation of a NaCl-triggered 0.5 wt% NapFF hydrogel by CSI. (a) ^1H image of sample. (b) ^2H-image of D_2O in sample taken immediately after (a) was recorded. (c) ^1H spectra extracted from (a) at vertical position indicated. (d) ^2H spectra of D_2O extracted from (b) at vertical position indicated.

The ^{1}H signal from the NMR-visible NapFF gradually diminishes as the concentration of NaCl increases towards the top of the image while there is a concomitant increase in the RQC of D_2O. These observations – in particular the lack of a clear diffusion 'front' as observed with $MgCl_2$ and $CaCl_2$ – suggest that the addition of NaCl does not induce changes in the sample as significant as those that take place upon the addition of $MgCl_2$ or $CaCl_2$. It has previously been demonstrated that 'gels' formed upon the addition of NaCl to 0.5 wt% solutions of NapFF are very much weaker than those formed with $MgCl_2$ or $CaCl_2$.

6. Analysis of NapFF hydrogels and solutions by polarised optical microscopy

Optical micrographs of NapFF hydrogels and solutions were collected in transmission mode on a Nikon Eclipse LV100 microscope equipped with an Infinity 2 colour CCD camera (Lumenera Corporation, Ontario, Canada). The samples were contained in 5 mm NMR tubes which were mounted on a glass slide.

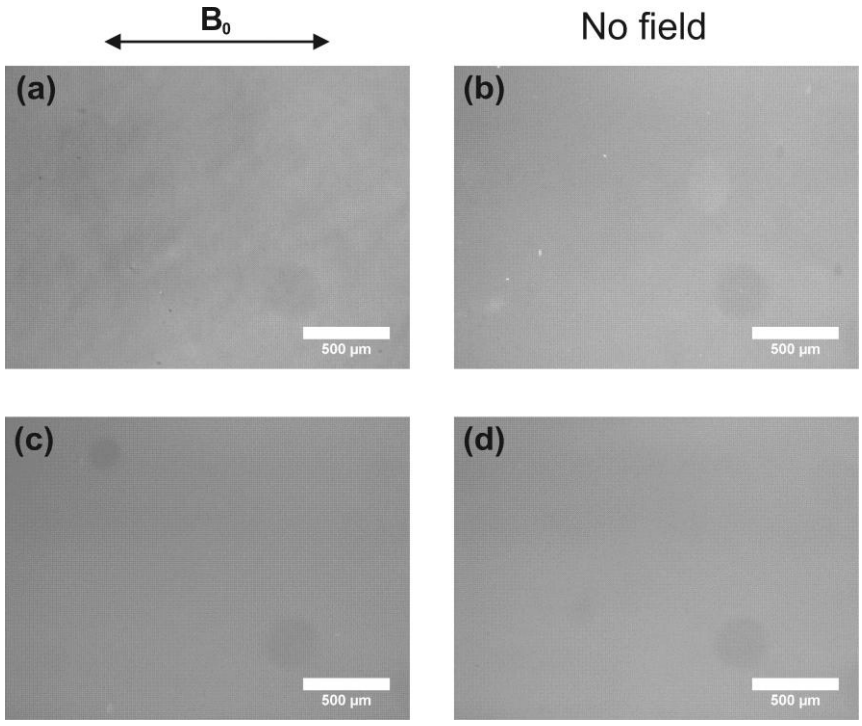

Figure S16. Analysis of 0.5 wt% NapFF hydrogels by polarised optical microscopy. All images were taken with the sample in a 5 mm NMR tube between crossed polarisers. The gels on the left hand images were formed in a 9.4 T magnetic field with the axis of the field indicated. The images on the right are of gels formed away from the magnetic field; the gels had not been exposed to a magnetic field before these images were recorded. (a-b) GdL-triggered hydrogels. (c-d) $CaCl_2$-triggered hydrogels.

Here, none of the gels prepared at 0.5 wt% exhibit birefringence, with no apparent difference between gels formed in and away from the magnetic field. It can be inferred that although the gels prepared in the magnetic field are aligned, as demonstrated by NMR spectroscopy, there is not enough material at 0.5 wt% to give appreciable birefringence. We note that solutions of NapFF at 0.5 wt% do sometimes contain birefringent domains; however, this effect seems very sensitive to the

temperature at which the solutions are prepared, stored and imaged, and will be the subject of future investigations. However, all samples exhibited alignment by NMR.

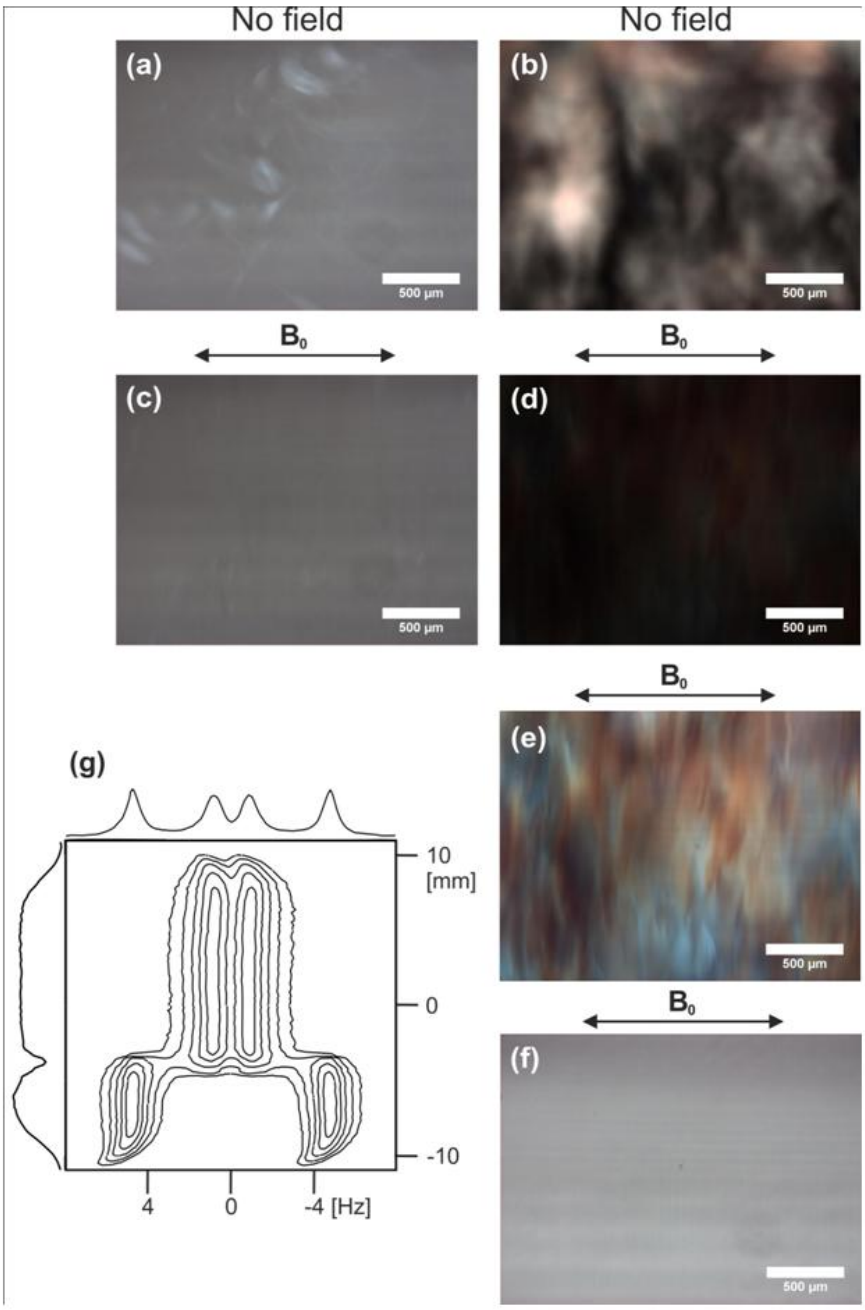

Figure S17. Analysis of a 1 wt% solution of NapFF by polarised optical microscopy. Images (a) to (e) were taken with the sample in a 5 mm NMR tube between crossed polarisers. (f) was taken without crossed polarisers. (a) and (b) were recorded before a magnetic field had been applied to the sample while (c) to (f) were recorded after exposure to a 9.4 T magnetic field for one hour. (g) is a ^{2}H image of D_2O in the sample demonstrating the existence of two regions (*vide infra*). The lateral stripes apparent on images (a), (c) and (f) are an optical effect due to the presence of an internal reference capillary in the sample.

At 1 wt%, NapFF forms liquid crystalline phases. A 1 wt% NapFF solution was prepared and placed in a 5 mm NMR tube along with a standard capillary. The liquid crystalline phases over time (8 days) seemingly sink to the bottom of the sample giving a densely birefringent region in the lower part of the tube (b) and a less birefringent region (a) in the upper region of the sample. ^{2}H-imaging of the sample (g) reveals that the RQC of D_2O is very different in the two regions, being very much larger in the more birefringent region. Upon exposure to a magnetic field for one hour, the birefringent domains become a lot less apparent in both the upper (c) and lower (d) regions. Care was taken to ensure that (a) and (c), and (b) and (d) were recorded under the same brightness. Upon increasing the brightness in the lower region (e), domains are apparent which seem to have a net alignment perpendicular to the axis of the magnetic field. The birefringent domains in the lower region are not apparent without crossed polarisers (f). These images suggest a 1 wt% solution of NapFF contains randomly oriented domains prior to magnetic field exposure, whereupon the domains align perpendicular to the magnetic field.

7. Analysis of hydrogels by FTIR

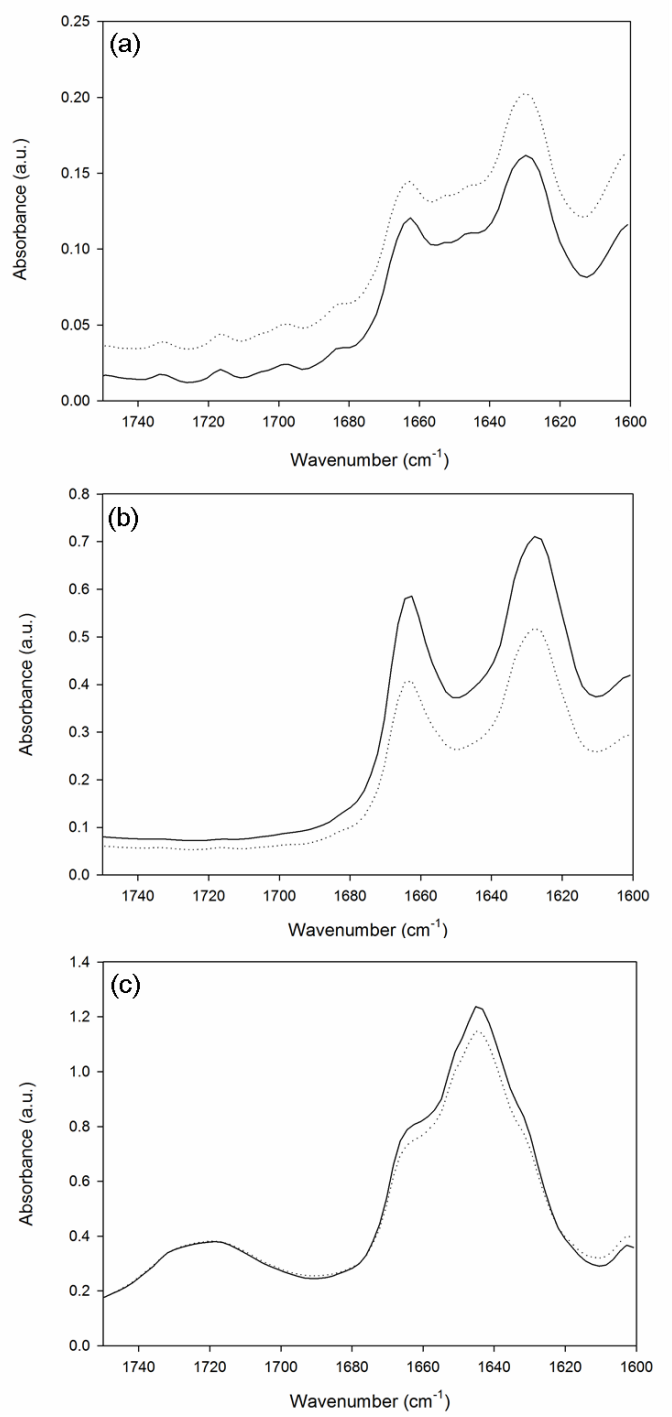

Figure S18. Analysis of magnetically aligned and non-magnetically aligned NapFF solutions and gels by FTIR. Spectra of magnetically aligned samples are shown with solid lines and non-magnetically aligned samples are shown with dashed lines. (a) Freshly mixed 0.5 wt% NapFF solutions. (b) $CaCl_2$-triggered hydrogels. (c) GdL-triggered hydrogels.

No difference is apparent between the magnetically aligned and non-magnetically aligned samples, suggesting that magnetic alignment does not significantly alter the supramolecular organisation of the peptides in the self-assembled aggregates.

8. Analysis of magnetically aligned and non-magnetically aligned $CaCl_2$-triggered hydrogels by SEM.

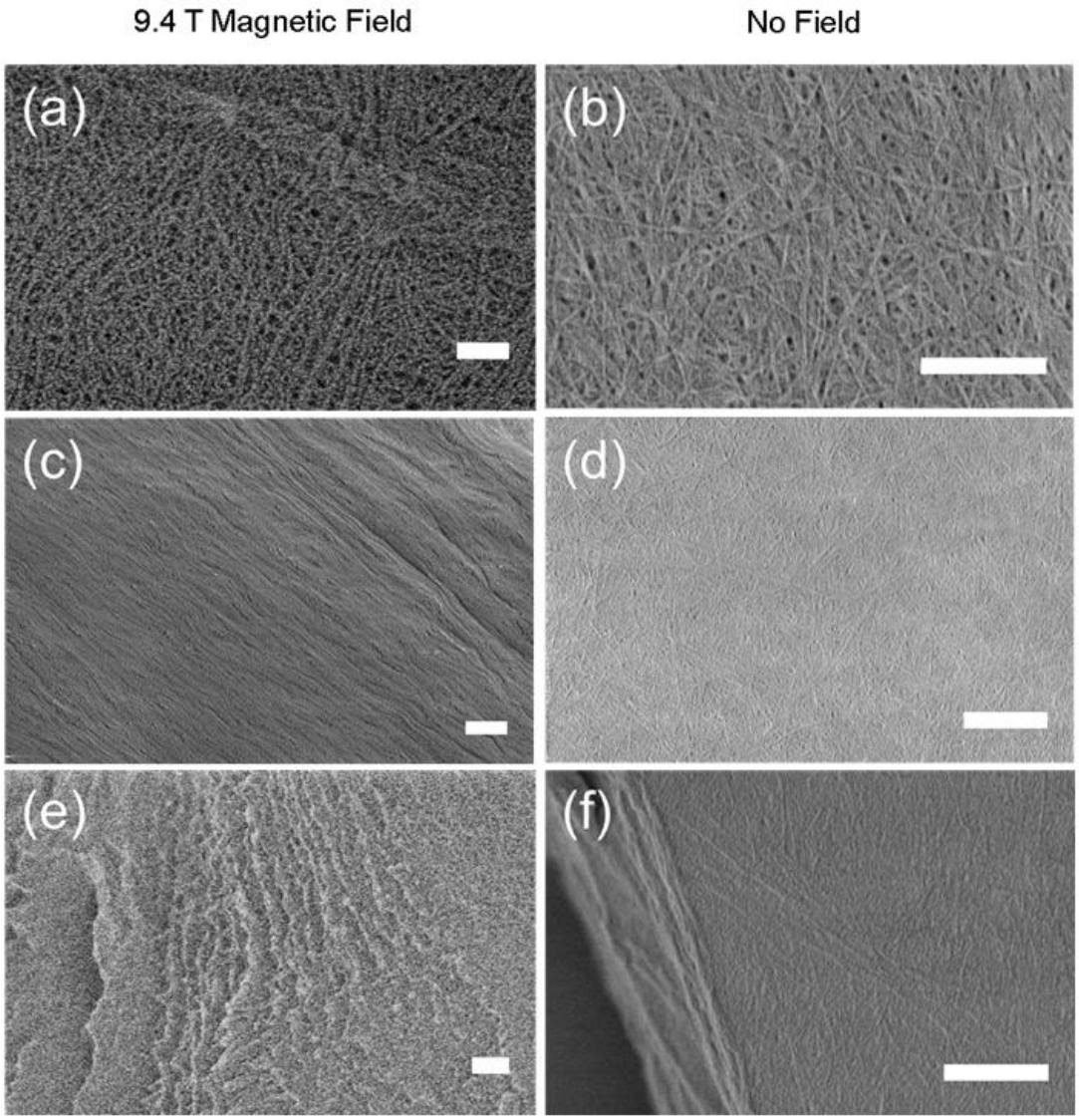

Figure S19. Side by side comparison of $CaCl_2$-triggered hydrogels gelled in a 9.4 T magnetic field (left) and with no magnetic field applied (right). (a,b,e,f) Scale bars = 500 nm. (c,d) Scale bars = 1 μm.

The fibres in the gel prepared in the 9.4 T magnetic field appear more aligned than the fibres in the gel prepared away from the magnetic field. The gels were dried so that the top surface of the gel lay perpendicular to the axis of the magnetic field during the formation of the gel prepared at 9.4 T. It was not possible to obtain good images of GdL-triggered hydrogels due to severe drying artefacts.

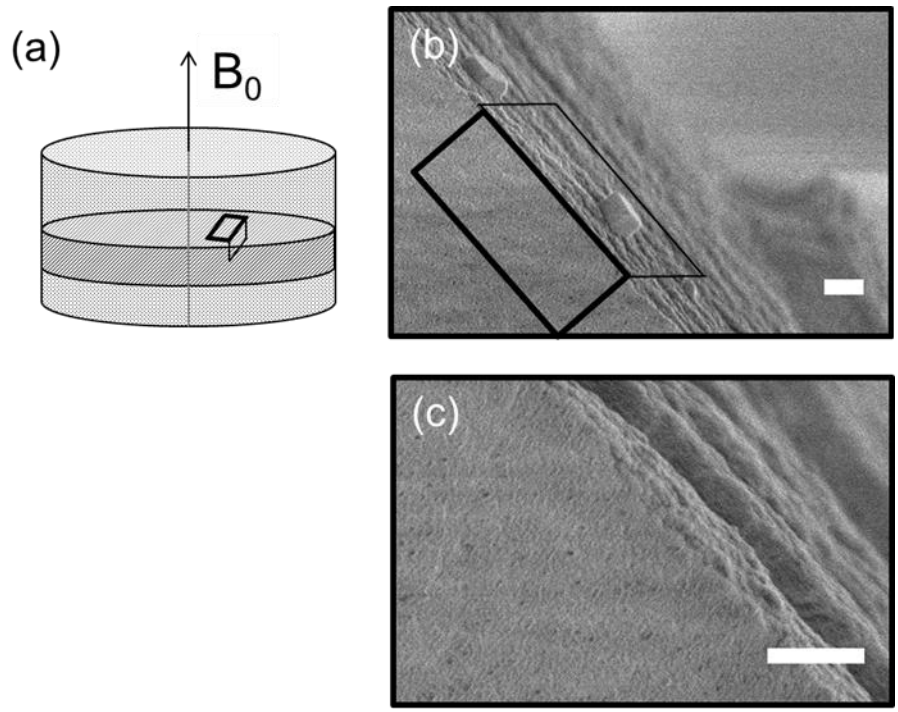

Figure S20. Cross-section at a fractured edge of a magnetically aligned $CaCl_2$-triggered hydrogel portion in the magnetic field. (a) Scheme to outline the coordinates of the magnetic field with respect to the SEM images (rectangle with thick line) and the fractured edge visible at a top view (rectangle with thin line). (b) SEM perspective of the edge from the plane perpendicular to the magnetic field (left) and the plane parallel to the magnetic field (right) with the presence of two crystals formed upon drying, possibly calcium chloride crystals; (c) Higher magnification at the fractured edge shows the dried fibrils aligned with the direction of view and layered films in the direction of the magnetic field, suggesting the hydrogels might have aligned bundles of fibers as it is packed in the dried state. Scale bars are 500 nm.

9. Powder X-ray Diffraction

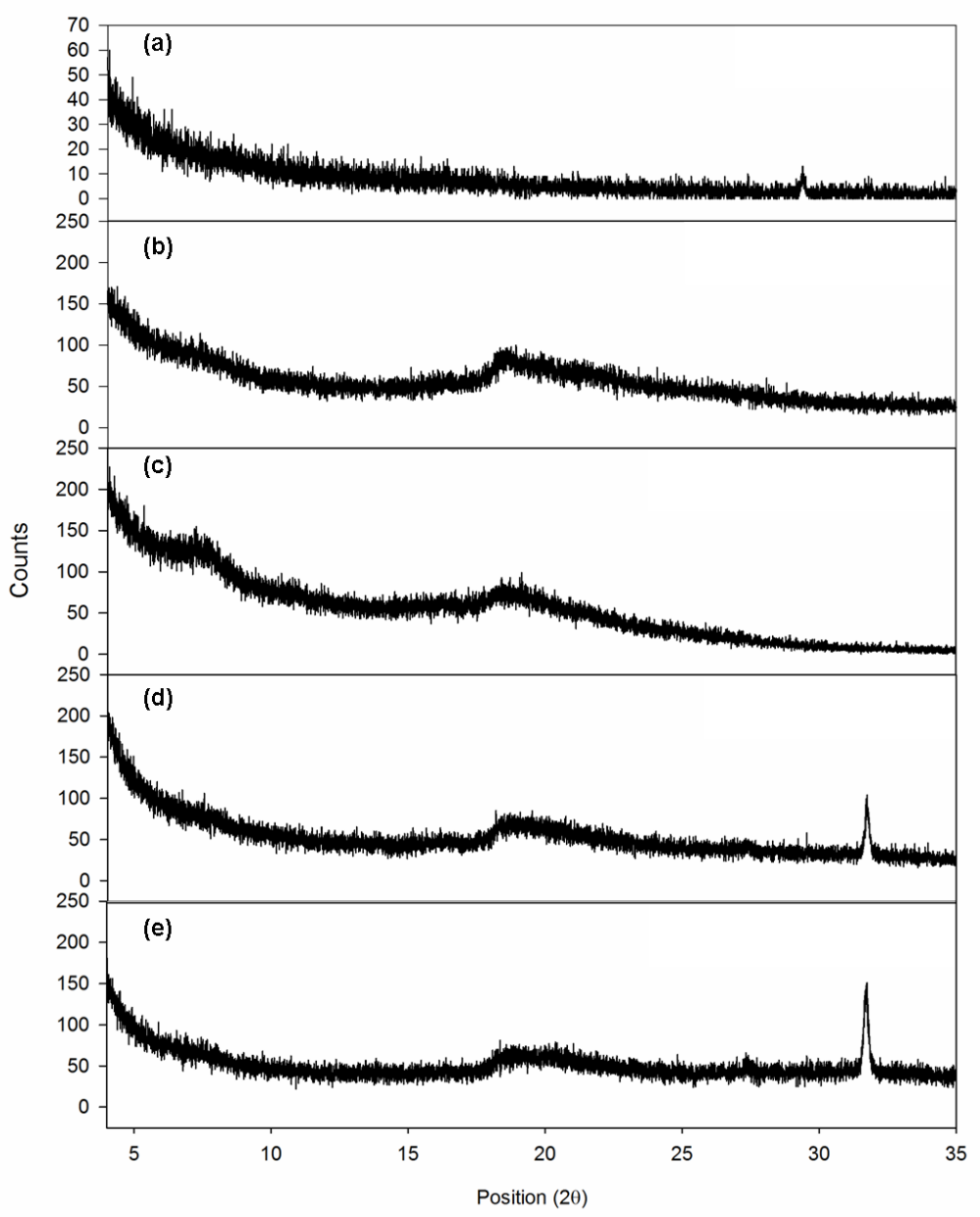

Figure S21. Powder XRD analysis of magnetically aligned and non-aligned $CaCl_2$ and GdL-triggered hydrogels. (a) Dried solution of 0.05 M $CaCl_2$ and 0.012 M NaOH. (b) Magnetically aligned GdL-triggered hydrogel. (c) Non-magnetically aligned GdL-triggered hydrogel. (d) Magnetically aligned $CaCl_2$-triggered hydrogel. (e) Non-magnetically aligned $CaCl_2$-triggered hydrogel.

The sharp peak in the pattern of the $CaCl_2$-triggered hydrogels can be identified with calcium salts. The gels appear amorphous by powder X-ray diffraction.

10. Other Gelators

Analogous data for a related gelator, 3MeO-FF, which also forms worm-like micelles at high pH.[6]

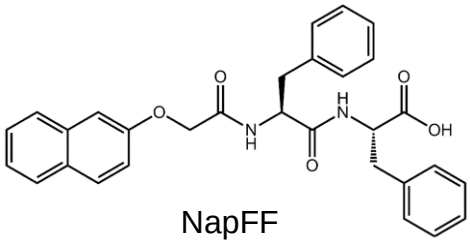

NapFF

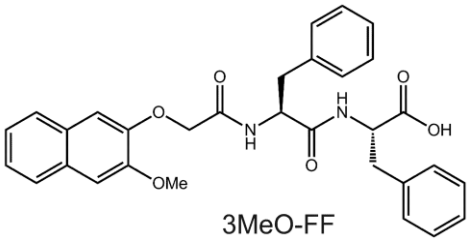

3MeO-FF

A solution of 3MeO-FF was prepared and $CaCl_2$ solution added following the same procedure used for NapFF. Formation of a $CaCl_2$-triggered 3MeO-FF hydrogel was then followed by CSI.

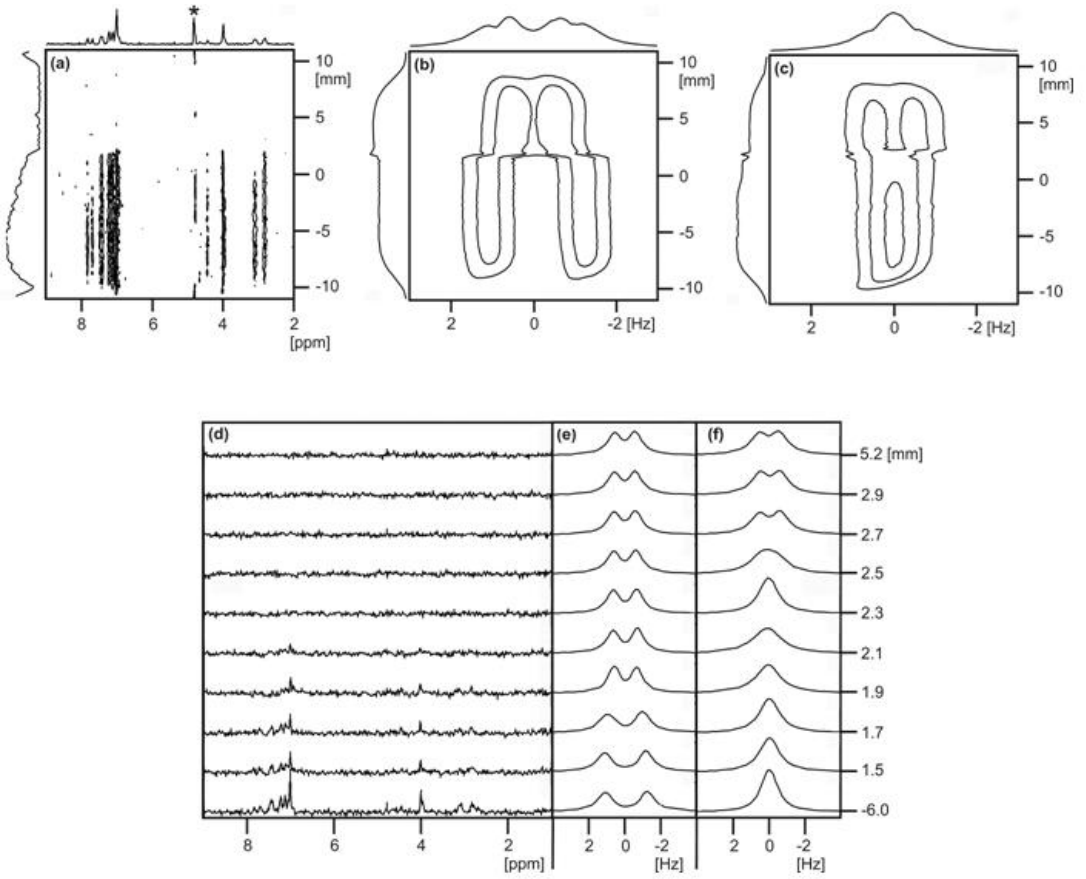

Figure S22. Following the formation of a $CaCl_2$-triggered 3MeO-FF hydrogel by CSI. (a) ^1H image of the sample. The residual signal from HOD is marked *. All other resonances belong to 3MeO-FF. (b) ^2H image showing D_2O resonance in sample taken immediately before removal from magnetic field. Acquisition of this image was started six minutes after (a) had completed. (c) ^2H image showing D_2O resonance in sample after ageing away from magnetic field for two weeks. (d) Extracted ^1H spectra from (a) at vertical positions indicated on left of figure. (e) Extracted ^2H spectra from (b) at vertical positions indicated. (f) Extracted ^2H spectra from (c) at vertical positions indicated.

In contrast to the case with NapFF (Fig. S7), the RQC of D_2O does not diminish to zero at approximately the same position that the signal from the NMR-visible gelator – measured as 20% of the total gelator present – vanishes (a), (d); however a noticeable discontinuity exists (e), the RQC decreasing abruptly between 1.7 and 1.9 mm. In the aged gel sample (c), (f), an RQC is detectable in the upper part of the gel which was gelled in the magnetic field; however, unlike with NapFF, no RQC is

detectable in the region gelled away from the magnetic field. These observations indicate that 3Meo-FF and NapFF may form different structures at high pH which may respond differently to the addition of $CaCl_2$ despite the structural similarity of the two gelators.

In contrast, Br-AV cannot be used to form $CaCl_2$-triggered gels. Br-AV does not form worm-like micelles at high pH.[6]

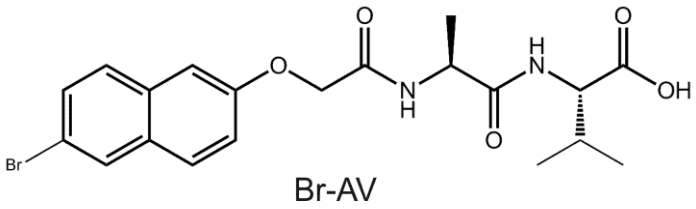

Br-AV

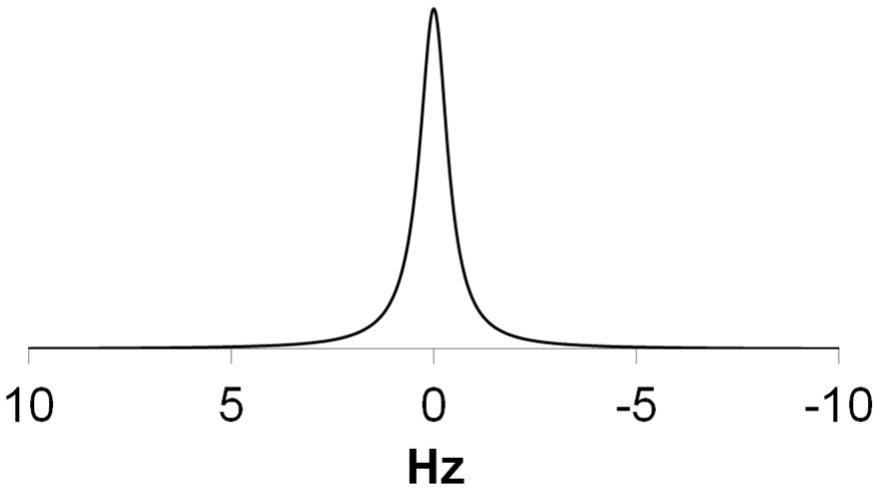

Figure S23. ^{2}H-NMR spectrum of D_2O in an 0.5 wt% solution of Br-AV at pD 12.1±0.1, aged for seven days.

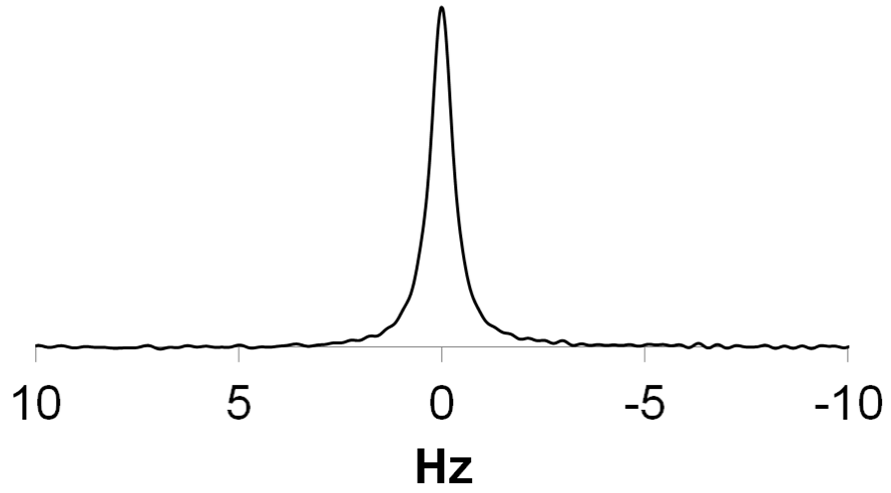

Figure S24. ^{2}H-NMR spectrum of dioxane-d_8 in an 0.5 wt% solution of Br-AV at pD 12.1±0.1, aged for seven days.

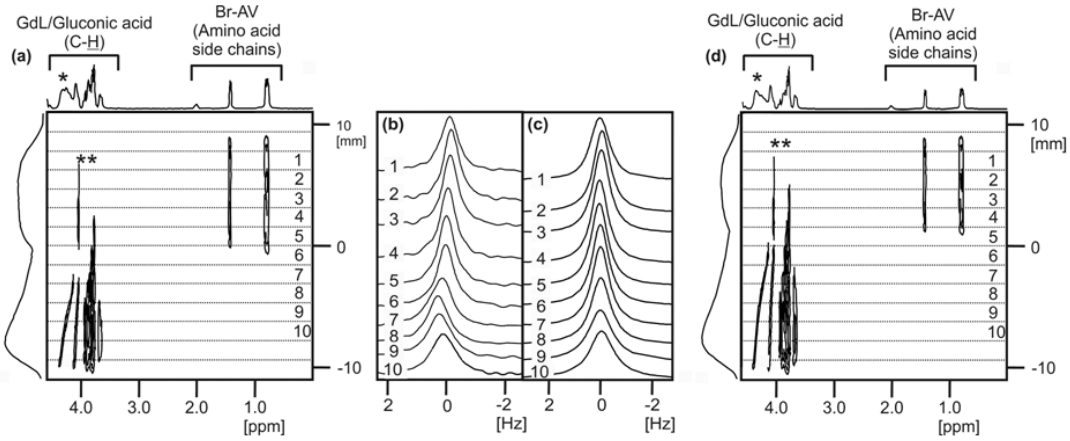

Figure S25. Following the formation of a GdL-triggered Br-AV gel by chemical shift imaging (CSI). Unlike the case with NapFF, when the GdL crystals were placed on top of the Br-AV solution, they promptly sank to the base of the NMR tube due to the much lower viscosity of the solution as compared to analogous NapFF solutions.[6] Diffusion of GdL/gluconic acid therefore took place upwards form the base of the NMR tube. (a) ^{1}H image of sample to show GdL/gluconic acid and Br-AV peaks. As above, the peak marked * can be used to estimate the pD. The peak marked ** belongs to Br-AV. As the Gdl/gluconic acid diffuses up the tube, the peaks from the NMR-visible gelator – measured as 100% of the total gelator present in analogous 0.5 wt% solutions of Br-AV – disappear indicating hydrogel formation. Image was recorded before (b). (b) ^{2}H-NMR spectra of dioxane-d_8 at regions indicated on (a). (c) ^{2}H-NMR spectra of D_2O at regions indicated on (a) recorded before (b). (d) ^{1}H-image of sample taken after acquisition of (b) and (c) showing how far the diffusion of GdL had progressed since (a) was recorded.

Neither dioxane-d_8 nor D_2O exhibit an RQC at any stage of the transformation from a solution at high pD to a GdL-triggered gel suggesting that worm-like structures capable of aligning in the magnetic field are not present. (b) and (c) were recorded with 16 gradient steps giving a spatial resolution of 1.6 mm. (b) was recorded with 256 scans and 3072 data points giving a total acquisition time of 4 hours.

11. Effect of ageing on solutions of NapFF at pD 12.6

In order to investigate the effect of ageing on solutions of NapFF at high pD, a sample of NapFF was prepared and placed in 5 mm NMR tubes which were stored between 18 and 20°C. Periodically, a tube was taken from storage and the splitting of the D_2O resonance measured. A plot of the splitting of the D_2O resonance versus the age of the sample reveals that the splitting reaches a plateau after six days. Optical micrographs of a sample between crossed-polarisers show how a nematic texture – indicative of the association of long fibrillar structures[7] – develops over the same time period and has stabilised after six days. The data presented here is in complete agreement with measurements of the viscosity of NapFF solutions presented elsewhere.[6] Images were collected as discussed in Section 6.

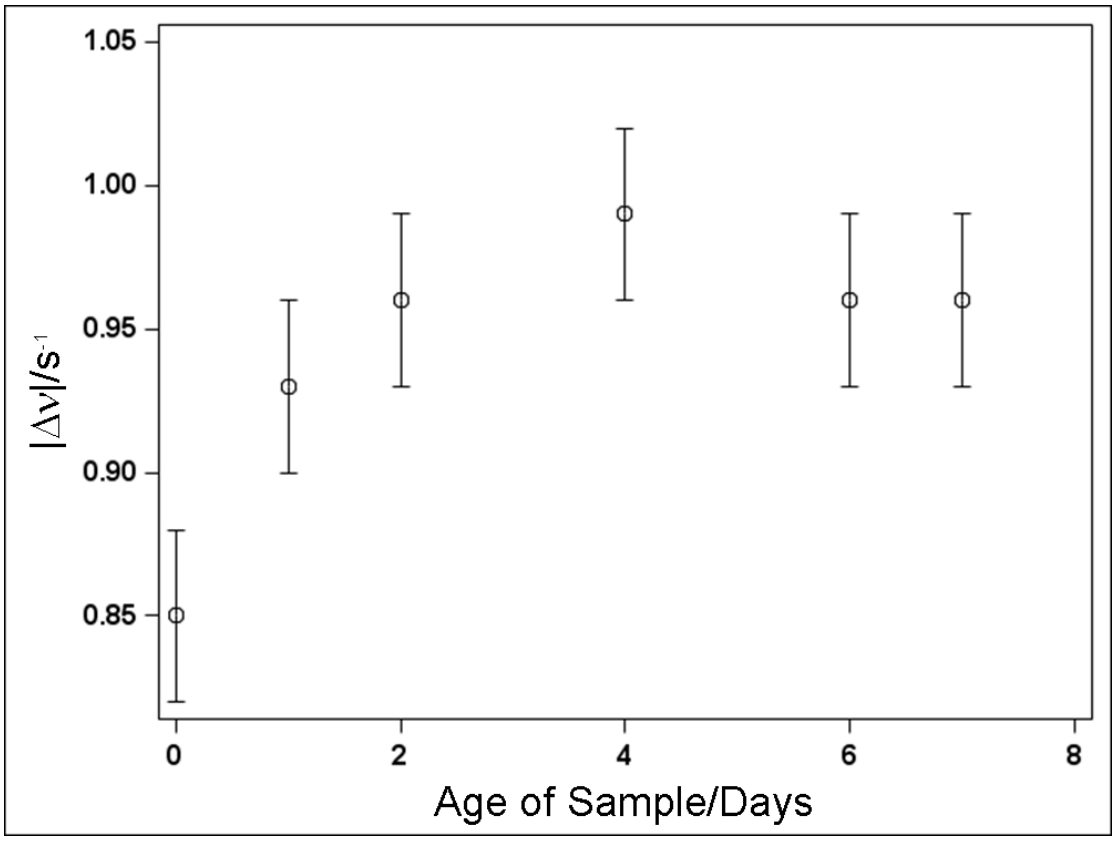

Figure S26. Plot of the RQC of D_2O ($|\Delta\nu|$) versus the age of the sample of NapFF. 0 days corresponds to a freshly mixed solution which has been stirred for 24 hours following the addition of D_2O and NaOD to solid NapFF. A standard error in $|\Delta\nu|$ of ±0.03 Hz has been assumed.

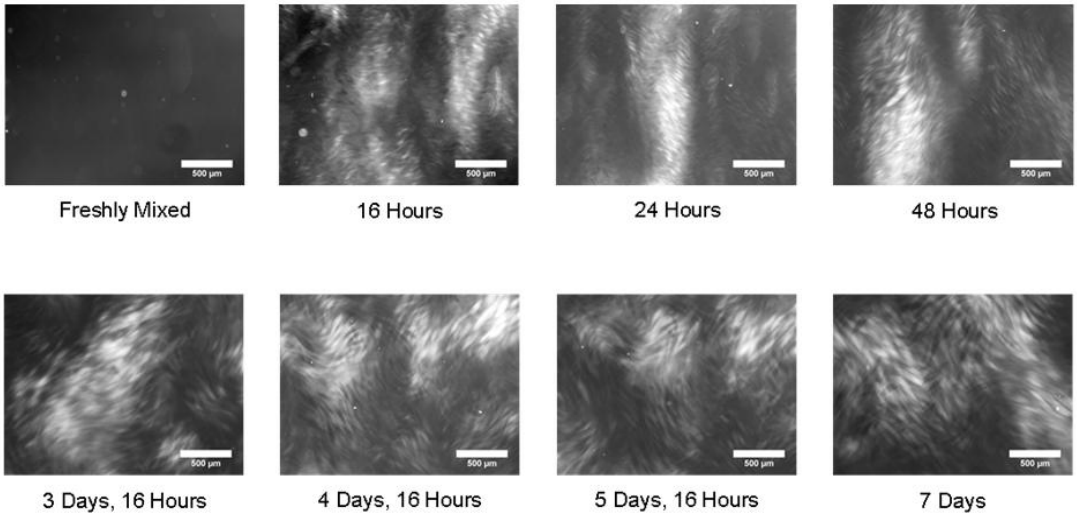

Figure S27. Optical micrographs of sample, taken between crossed-polarisers, of age indicated. Samples had not been exposed to a magnetic field before these images were taken.

12. Additional confocal microscopy images of $CaCl_2$-triggered gels prepared in the presence and absence of a magnetic field

Samples for confocal microscopy analysis were prepared according to the procedure described in Section 1 which allowed imaging of the sample in planes perpendicular and parallel to the direction at which the 9.4 T magnetic field had been applied to the sample gelled in the field.

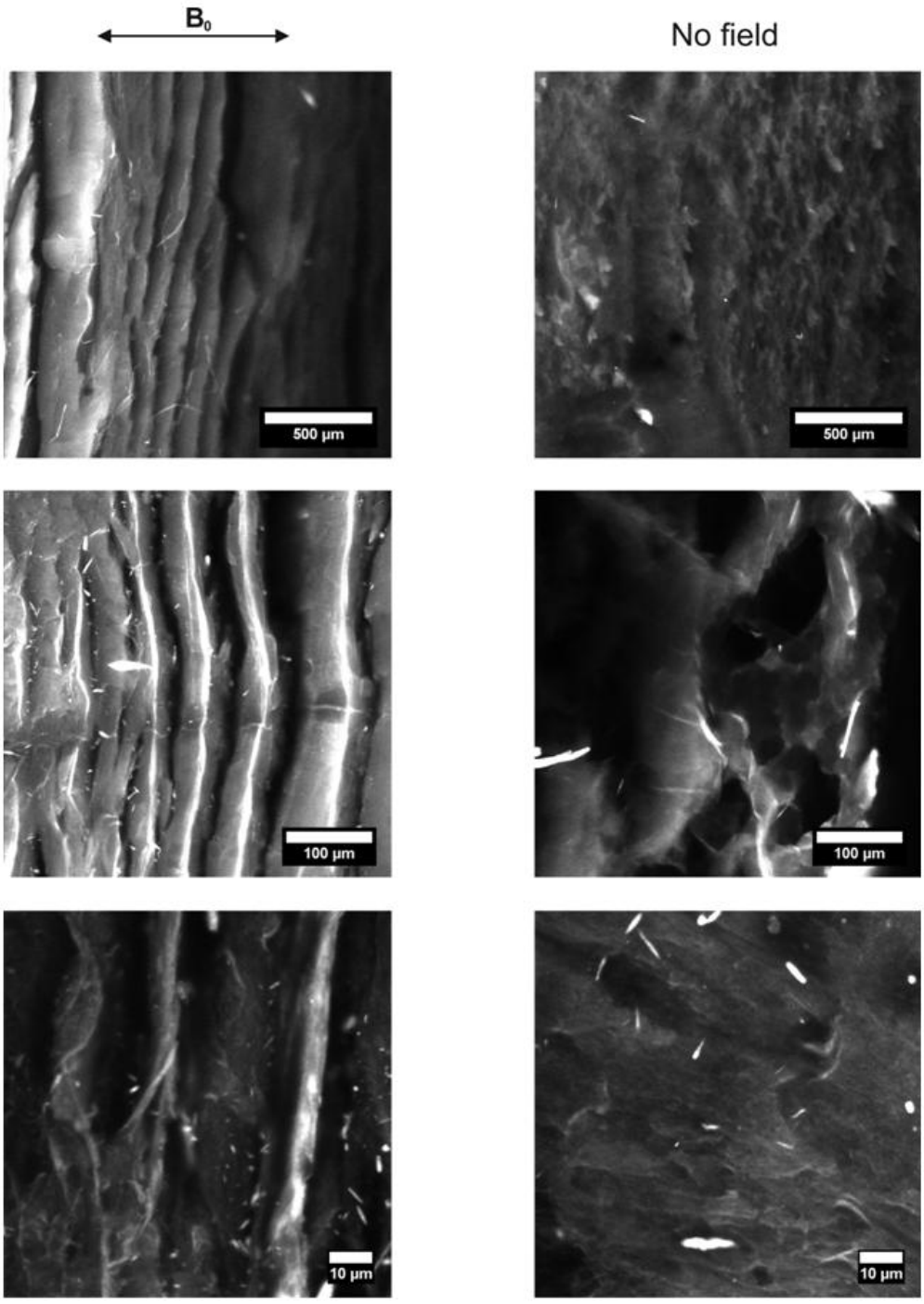

Figure S28. The images on the left are of the sample prepared in a 9.4 T field, with the axis of the field with respect to the focal plane indicated. Images on the right are of gels formed away from the magnetic field.

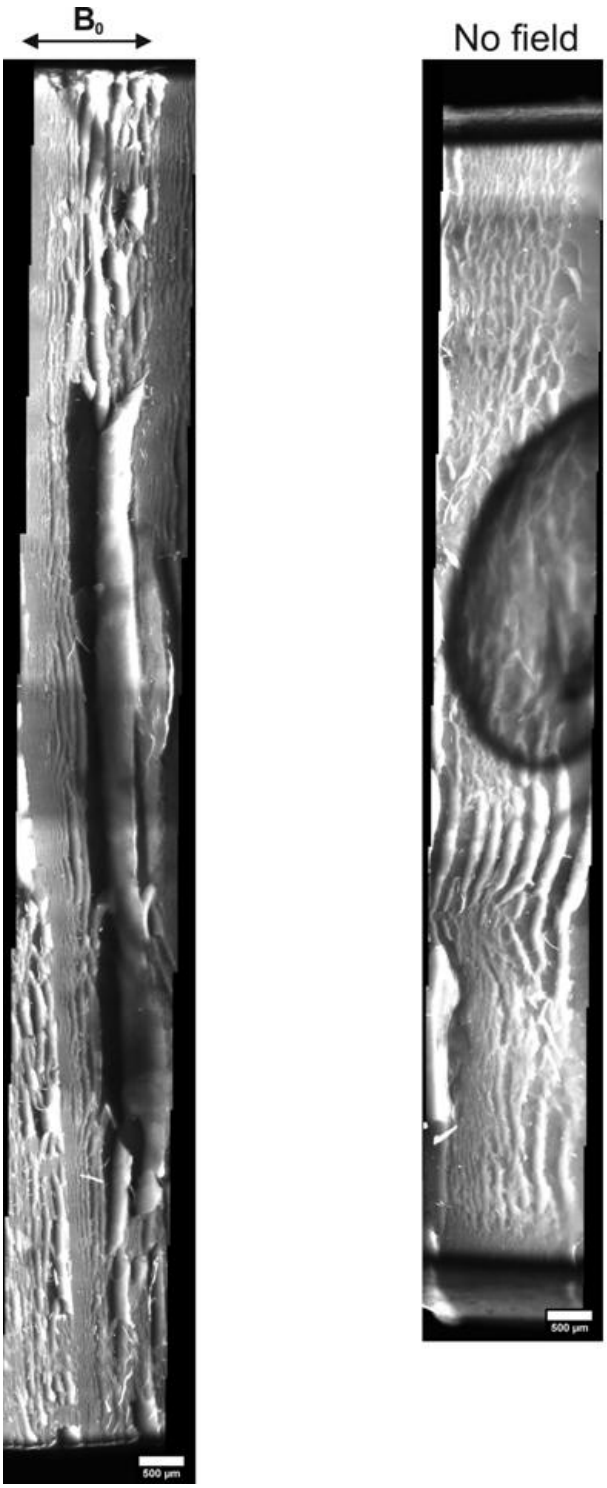

Figure S29. Composite images comprising individual images which have been fused together to form a complete image of the sample. The large round object on the image

of the sample prepared away from the magnetic field is an air bubble which was trapped when mounting the sample for confocal microscopy.

References

1. P. Trigo-Mouriño, C. Merle, M. R. M. Koos, B. Luy and R. R. Gil, *Chem. Eur. J.*, 2013, **19**, 7013-7019.
2. A. Pallagi, P. Sebők, P. Forgó, T. Jakusch, I. Pálinkó and P. Sipos, *Carbohydrate Research*, 2010, **345**, 1856-1864.
3. L. Chen, S. Revel, K. Morris, L. C. Serpell and D. J. Adams, *Langmuir*, 2010, **26**, 13466-13471.
4. A. Delville, J. Grandjean and P. Laszlo, *Journal of Physical Chemistry*, 1991, **95**, 1383-1392.
5. L. Chen, G. Pont, K. Morris, G. Lotze, A. Squires, L. C. Serpell and D. J. Adams, *Chemical Communications*, 2011, **47**, 12071-12073.
6. L. Chen, T. O. McDonald and D. J. Adams, *RSC Advances*, 2013, **3**, 8714-8720.
7. J. V. Selinger and R. F. Bruinsma, *Physical Review A*, 1991, **43**, 2922-2931.